Chapter 16
Nanotheranostics-Based Imaging for Cancer Treatment Monitoring

Tianxin Miao, Rachael A. Floreani, Gang Liu, and Xiaoyuan Chen

16.1 Introduction

Approximately 1.7 million new cancer cases were projected in the year 2017, recognized as the one of the primary health threats in the United States [1, 2]. Thus, cancer research is focused on developing effective strategies for cancer diagnosis, treatment, and monitoring treatment response [3]. Despite the progress in the past 20 years, early cancer diagnosis and effective treatment remain critical challenges [2, 4, 5]. Further, early detection of the therapeutic response in a treatment cycle would be beneficial for patients and insightful for physicians to gather the

T. Miao
Bioengineering Program, College of Engineering and Mathematical Sciences, College of Medicine, University of Vermont, Burlington, VT, USA
e-mail: Tianxin.Miao@uvm.edu

R. A. Floreani
Bioengineering Program, College of Engineering and Mathematical Sciences, College of Medicine, University of Vermont, Burlington, VT, USA

Mechanical Engineering Program, College of Engineering and Mathematical Sciences, University of Vermont, Burlington, VT, USA
e-mail: floreani@uvm.edu

G. Liu (✉)
State Key Laboratory of Molecular Vaccinology and Molecular Diagnostics & Center for Molecular Imaging and Translational Medicine, School of Public Health, Xiamen University, Xiamen, China
e-mail: gangliu.cmitm@xmu.edu.cn

X. Chen (✉)
Laboratory of Molecular Imaging and Nanomedicine, National Institute of Biomedical Imaging and Bioengineering, National Institutes of Health, Bethesda, MD, USA
e-mail: shawn.chen@nih.gov

P. Rai, S. A. Morris (eds.), *Nanotheranostics for Cancer Applications*, Bioanalysis 5, https://doi.org/10.1007/978-3-030-01775-0_16

information required to determine if an alternative therapeutic method is needed in cases where the current approach is not working or no longer works.

The field of biomaterials has enabled researchers to develop novel strategies to assist disease diagnosis and monitoring [6, 7], anticancer drug delivery [8, 9], and tissue regeneration [10–12]. The use of nanotechnology in medicine, also referred to as nanomedicine, has been widely applied in the field of biomedicine, especially in cancer therapy, which is an appealing and versatile strategy for selective drug delivery and diagnostics [13]. Nanotechnology refers to the fabrication of materials with dimensions between 1 nm and 100 nm [3, 14], capable of achieving high concentrations in targeted tissue locations [15]. With the development of nanotechnology, nanomedicine holds potential to integrate both diagnostic and therapeutic functionalities into one single material/application, playing a critical role in cancer therapy [14].

Recently, the idea of personal treatment monitoring has gained attention, providing a means to evaluate treatment effectiveness while protecting patients from adverse drug effects [16]. The goal of detecting early signs of response is to predict the possible outcome of treatment in general as well as to identify potential predictive markers of response. The collection of such data will help physicians identify patient groups that are most appropriate for a specific therapy. Markers of response could include, for example, apoptosis or changes in metabolism (glycolysis or amino acid or lipid metabolism) or receptor expression associated with tumor cell death or inhibition of proliferation or inducing cell death, whereas predictors of response may include the expression of, say, hormone receptors, which predict response to anti-hormonal treatment, or microRNAs, or the presence of tumor hypoxia, which can affect the effectiveness of certain treatments like radiation therapy or photodynamic therapy.

The most common technology utilized for treatment monitoring is molecular imaging, defined as "in vivo imaging and characterization of biologic processes at the cellular/molecular level in a noninvasive way," which provides comprehension into both cancer diagnosis and therapeutic response monitoring [2, 17]. The term "theranostics" is now emerging due to the exceptional ability of nanoplatforms to load both imaging and therapeutic cargos, resulting in multifunctional combined nanosystems able to simultaneously detect early signs of cancer, deliver drug, and monitor therapeutic response. Indeed, nanotheranostics (i.e., theranostic nanomedicines) that incorporate imaging and therapeutic functions into a single system (i.e., nanoparticles) provide the ability to monitor drug release and circulation in real time and to predict and certify the effectiveness of cancer therapies [13]. The field of nanotheranostics is growing due to increasing medical needs, including those in the fields of cancer therapy and personalized disease treatments [18, 19]. Furthermore, theranostic nanoparticles have been developed to integrate disease diagnosis, targeted delivery, controlled drug release, and drug monitoring into a unifying platform. In combination with advanced techniques in different imaging instruments, nanoparticles with multimodal imaging capabilities have the potential to offer higher-quality images at multiple length scales and different clinical stages and offer more precise disease diagnosis and monitoring. The advantages of

nanotechnology are that particles can be designed and fabricated with controllable size, shape, and composition, as well as physical properties [19]. The high ratio of surface area to volume for nanomaterials contrary to traditional macroscopic materials also makes it a desirable choice for nanotheranostics [20]. In addition, they can be easily modified through different bioconjugation techniques to enhance the functionalities. An important class of nanoparticles is made of inorganic materials, such as metal [21], metal oxide [22], semiconductors [23], or even rare earth minerals or silica [24]. Organic nanoparticles have also been prepared using various biodegradable polymers such as polylactide-polyglycolide [25] and polycaprolactones [26], as well as proteinaceous materials, such as albumin [27] and collagen [28].

Convincing arguments have been made in the field of cancer therapy monitoring in favor of developing nanoprobe-based, imaging-guided therapy [29–31]. First, revealing the early response of tumors in regard to treatment may provide insights into selecting the most appropriate therapeutic method, offering benefits for patients and for healthcare systems [31]. In a large randomized controlled trial performed by the National Lung Screen Study (NLST), researchers reported that chest radiographs were less efficient in identifying lung cancer among older and former heavy smokers compared to low-dose computed tomography (CT) [32]. This is because in CT, X-ray has a circular movement around the body, allowing a variety of views of the same tissue compared to traditional chest radiographs [33]. This initial large clinical study showed higher efficacy in screening for lung cancer with CT compared to prior trials using sputum cytology and chest radiographs. Now that CT screening has been shown to be effective, more use of this type of screening shall become the next step. Second, imaging techniques allow doctors to monitor the biochemical and cell biology aspects of tumors, providing early indications of whether how and when tumors respond to treatments [31]. Third, with properly labeled cell metabolites or receptor ligands, radionuclide imaging techniques, such as positron-emission tomography (PET) and single-photon emission computed tomography (SPECT), can be applied to monitor tumor metabolism or receptor expression levels of target cancer cells [31]. Fourth, other imaging techniques such as magnetic resonance imaging (MRI) could not only provide high-resolution images of tissue morphology but also cancer cell receptor expression with the assistance of paramagnetic nanomaterials labeled with receptor-targeting ligands [31]. Different imaging techniques have their own advantages in various imaging scenarios. With the advantages of different imaging techniques, we are capable of obtaining images from tissue morphology to cellular metabolites, which have helped to better serve the purpose of treatment monitoring referred to as “nanotheranostics.”

This chapter will focus on the treatment monitoring aspects of nanotheranostics with detailed introduction on application of treatment monitoring in cancer therapy, including MRI [34], PET [35], SPECT [36], and optical imaging [37] since these techniques have been widely applied in the area of treatment monitoring with an extended detection limit for molecular imaging. There is also research on computed tomography (CT) nanoparticles with clinical application of identifying the metastatic lesions on lung cancer [38].

With the development of imaging techniques, clinicians and researchers are not satisfied with visualizing the tumor tissue alone, but are also looking to explore the molecular aspect of the tumor microenvironment. In addition, certain cellular kinase/enzymatic reaction and gene expression will also be invaluable information obtained from molecular imaging. For example, acquiring information on angiogenesis will provide early cancer detection prior to the formation of a solid tumor. The monitoring of metastasis for single circulating cancer cells will enable physicians to initiate a preventive care regimen as early as possible. As biomedical researchers, we are continuously interested in improving the detection and therapeutic monitoring of cancer disease. Therefore, there is a great need to study molecular imaging for therapeutic monitoring in cancer with respect to pathological conditions such as angiogenesis and apoptosis.

16.2 MRI

MRI is a widely used, noninvasive imaging technique offering the possibility of penetrating into soft tissue and great spatial-temporal resolution associated with relative ease of operation procedures [39, 40]. The principle of MRI is similar to that used in chemical nuclear magnetic resonance (NMR) analysis, in which the spins of specific atomic nuclei are visualized within the body [41]. The altered T_1 (longitudinal) and T_2 (transversal) proton relaxation times within various tissues generate autogenous contrast [13]. Generally, increased water content as well as the inflammation/tumor site has a relatively black/dark signal on T_1-weighted images while relative white/bright signal on T_2-weighted images, which identifies tumor tissue over normal healthy region [42]. In addition to its application in disease differentiation, disease diagnosis, and therapy monitoring, MRI is also exploited in nanomedicine research, in order to (1) perform pharmacokinetics and biodistribution analyses, (2) monitor drug release, and (3) enable cell tracking studies. MRI has been integrated into almost every aspect of cancer clinical practice, including diagnosing, assisted-surgery and radio−/chemotherapy monitoring, and so on. In general, MRI assists cancer treatment mainly in the following aspects: first, the high soft tissue resolution of MRI makes it an important tool for delineating, staging, and monitoring treatment efficacy of cancer; secondly, real-time MRI utilizing various physiological parameters including temperature, water content, and pH also provides invaluable insight on anticancer therapy; thirdly, nanoparticles with combined functional groups and targeting moieties are being designed and fabricated to meet the dual purpose of cancer care—diagnosing/monitoring and treatment [43].

Despite being a highly useful and broadly applicable modality for clinical diagnosis and therapy monitoring, several disadvantages are associated with MRI in treatment monitoring, including (1) relatively low contrast agent sensitivity, (2) relatively difficult quantification procedures, and (3) the time and cost involved. To overcome these limitations, nano-based MR contrast agents, as opposed to radionuclides, could offer optimal conditions for assessing drug release due to access to freely diffusing water molecules to generate contrast and, therefore, render

different signals when present within vs outside of nanocarriers [41]. This type of technique has been widely applied in cancer treatment monitoring.

As stated above, by calculating the T_1 longitudinal relaxation and the T_2 transversal proton relaxation time, images are generated by organs within the human body. The two separate types of signals introduce two different categories of MRI contrast agents into T_1 and T_2 [42, 44]. Commercially offered T_1 contrast agents are typically paramagnetic complexes, for instance, gadolinium (Gd)-related compounds including gadoterate and gadodiamide, whereas T_2 contrast agents are usually iron oxides, such as Feridex and Resovist [44]. Due to the different imaging signals of T_1 and T_2, the design of either T_1 or T_2 contrast agents is very different. Cancer tissue is brighter in T_1 and darker in T_2 compared to normal tissue. Therefore, T_1 contrast agents enhance the final signal images of tumor region; T_2-weighted contrast agents actually diminish signal intensity at the same location. The boosting development of nanotechnology saw a number of different nanomaterials generated from basic T_1 and T_2 contrast agents, including polymeric micelles, multifunctional nanoparticles, as well as liposomes often supplemented with basic components of contrast agents, such as iron oxide nanoparticles and paramagnetic metal ions [45–48]. Kaida et al. [49] reported an example of micelle-based MRI contrast agents. By utilizing multifunctional polymeric nanoparticles, anticancer drug platinum and the paramagnetic Gd were incorporated via reversible metal chelation reaction. The dual function system eliminated cancer in an orthotopic animal model of human pancreatic tumor while monitoring the therapeutic efficacy simultaneously [49]. Such polymeric micelles open exciting prospects for improving the management of cancer therapy [13]. Similarly, doxorubicin-loaded thermally cross-linked superparamagnetic iron oxide nanoparticles (Dox@TCL-SPION) is an example for T_2-weighted nanotheranostics. By conjugating doxorubicin on the PEG-coated SPION nanoparticles, this multitasking "rust ball" can answer the question of where a tumor is located, whether drugs are properly accumulated in the tumor area, and how the tumor responds to therapy [50]. In another example, Ng et al. reported the early CRLX101 therapeutic response in a mouse model used to study tumor cell proliferation. CRLX101 contains camptothecin, a DNA topoisomerase I inhibitor with additional polysaccharide (cyclodextrin) coating to form polymeric particles. The drug exhibited excellent early therapeutic effect with good monitoring resolution in a preclinical mouse model of malignant lymphoma using diffusion MRI. All examples above have revealed the potential of combining MRI contrast agents and therapeutics together as nanotheranostics for treatment monitoring in cancer [51]. In the following section, we will focus on utilizing MRI for specific tumor pathophysiology imaging, including angiogenesis, metastasis, and apoptosis.

16.2.1 MRI for Tumor Angiogenesis Imaging

One of the main driving forces for tumor formation is the deregulation of angiogenesis, defined as the development of new blood vessels. This is because the new growth of tissue would require nutrients and oxygen, which are delivered through

the newly grown blood vessels. In 1971, Judah Folkman first proposed the hypothesis of neoangiogenesis [52]. According to this hypothesis, the resting state of the mature endothelial cells can be switched to neovasculature by the activation of chemical signal molecules originated from the tumor cells. Positive regulators of angiogenesis, including vascular endothelial growth factor (VEGF), interleukin-8 (IL-8), fibroblast growth factor-2 (FGF-2), platelet-derived growth factor (PDGF), placental growth factor (PlGF), transforming growth factor-beta (TGF-β), and angiopoietins (Angs), were discovered to be involved in the transition [53]. Generally, these molecules can be transported outside tumor cells, assembled from the extracellular matrix or recruited by tumor. Up to now, angiogenesis has been recognized as one of the significant pathological features of cancer, enabling better diagnosis and treatment monitoring of metabolic deregulation and tumor metastasis [54].

Several main signal molecules that regulate tumor angiogenesis and cell adhesion include the VEGF/VEGF receptor signaling pathway and integrin $\alpha_v\beta_3$, which can be used as nanomaterial targeting agents that enhance efficacy by homing to the tumor vasculature [55]. Dynamic contrast-enhanced MRI has been used indirectly in measuring vascular permeability to provide insight on tissue perfusion and permeability of tumor vasculature [56, 57]. Researchers have attempted to link MRI parameters with VEGF expression by correlative analysis of tissue morphology, vascular density with CD31 marker, and vascular permeability [58]; however, this was not applicable in some of the reports [59]. Direct evaluation of VEGF/VEGFR expression by MRI without the use of contrast agents has not been achieved. Nevertheless, targeted ultrasound and optical imaging have reported VEGF/VEGFR imaging in the past few decades [60], which will be discussed in a later section.

The integrin signaling pathway plays an important role in tumor angiogenesis, cell migration, survival, and metastasis. Integrin $\alpha_v\beta_3$, in particular, is significantly upregulated on tumor microenvironment blood vessels but not on inactive endothelium [61]. Most imaging studies of $\alpha_v\beta_3$ integrins have used arginine-glycine-aspartic acid (RGD)-based probes to which integrins bind [61, 62]. Targeted contrast agents have incorporated Gd(III) chelates and targeting agents (i.e., RGD) via a direct conjugation reaction. Nevertheless, due to the low sensitivity of MRI and the relatively low concentration of integrin in targeted tissues, such directly conjugated contrast agents with MRI are not as effective as radionuclide imaging. Therefore, different types of carriers, including polymers, dendrimer, liposomes, and micelles, have been designed to deliver sufficient amount of Gd(III) to enhance tumor site MRI signal [63]. Liposomes with paramagnetic Gd^{3+} chelates at sizes of 300–350 nm in diameter were reported to image $\alpha_v\beta_3$ expression with MRI [64]. In the study, Sipkins et al. designed a novel approach to detect angiogenesis using MRI with $\alpha_v\beta_3$ monoclonal antibody in rabbit carcinomas. Significant tumor contrast was found in T_1-weighted images after injection of targeted liposomes but not control liposomes without conjugating targeting moieties [64]. These promising results have led to many other designs of nanocarrier-based MRI contrast agents for angiogenesis [65].

16.2.2 MRI for Evaluating Cancer Metastases

Evaluating the treatment effect in patients with metastatic cancer is very important in daily oncology practice, especially for patients with metastases to the bone, which are often difficult to detect. This difficulty is due to the nature and complexities of fixed bone defects, which range from sclerotic to osteolytic, as well as the low specificity, sensitivity, and spatial resolution of the previously available bone imaging methods, primarily bone scintigraphy. The process by which cancer cells infiltrate the bone marrow can be detected and quantified using morphological imaging with functional approaches, such as MRI or CT [66]. With the injection of cancer cells pre-labeled with iron oxide particles with diameter in micron into the left ventricle of a beating mouse heart, Heyn et al. were able to track exogenous cancer cells after transportation into the murine brain [67]. This approach allowed the imaging of the early delivery and distribution of cells, as well as new tumor tissue growing from a subset of these cells within the whole intact brain. The particle being used here was a commercially available micro-sized iron oxide and highlights the application of MRI to monitor the metastatic process during treatment [67]. More importantly, nanoparticles possess a large surface area for conjugation to several therapeutic and diagnostic agents and are able to pass the blood-brain barrier to reach the target cancer tissue [68].

16.2.3 MRI for Apoptosis

Apoptosis is a mechanism of programmed cell death that is activated during embryonic development, during the normal maintenance of homeostasis, and under pathological circumstances [69]. Successful cancer treatments, such as radiation [70], chemotherapy [71], thermal therapy [72], and photodynamic therapy [73], could induce apoptosis [74]. Imaging apoptosis will give doctors a general idea of when cancer cells start dying and the tumor starts shrinking. Considering the essential role of apoptosis, a robust imaging method is needed to detect and monitor this process. One of the initial biochemical events that occurs during the apoptotic process is the externalization of phosphatidylserine (PS) [75]. PS is normally constrained to the inner membrane layer. However, when PS is externalized, phagocytes recognize the cells initiating the apoptosis process. Apoptotic cells are phagocytosed by macrophages in a manner reliant on externalized PS prior to an increase in plasma membrane permeability. Thus, PS is an important marker for apoptosis and has been used as a potential cancer marker for MRI-based detection of apoptosis [76]. The surface PS can be detected with a human protein named annexin V in a Ca^{2+} dependent, which has been used in the design of molecular imaging probes. Jung et al. reported conjugation of biotinylated annexin V-glutathione onto streptavidin-conjugated SPIO or Gd chelate avidin could elevate T_2- and T_1-weighted MRI signal in detecting apoptotic murine lymphoma cells (Fig. 16.1) [77]. In addition, annexin

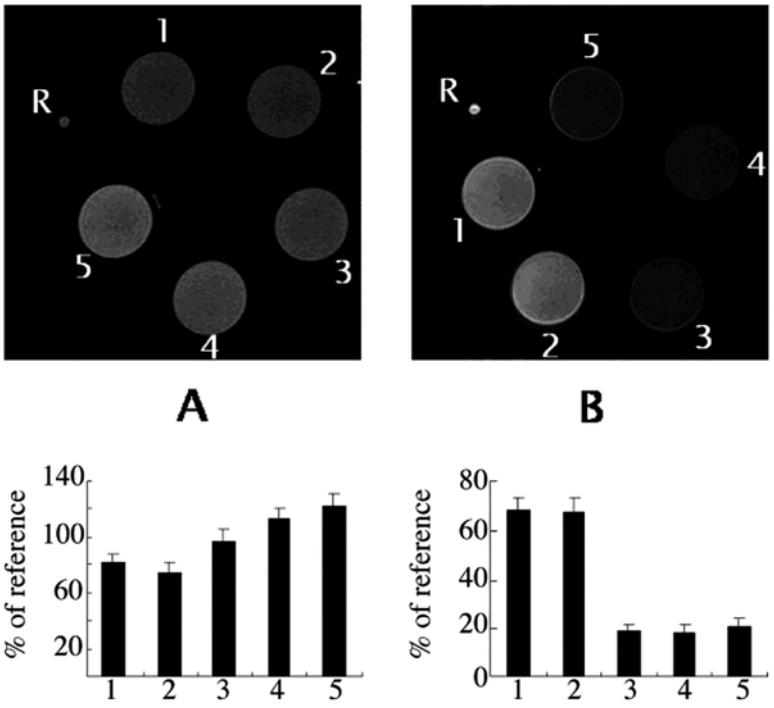

Fig. 16.1 MRI signal of PS-targeted contrast agents. (**a**) T_1- and (**b**) T_2-weighted MR imaging of apoptotic cells after incubation with biotin-annexin V at different concentrations and then subsequently incubated with avidin-GdDTPA or streptavidin-SPIO. (1) Pure apoptotic cells, (2) apoptotic cells with avidin-GdDTPA or streptavidin-SPIO. (3–5) Apoptotic cells with avidin-GdDTPA or streptavidin-SPIO with elevated biotin-annexin V concentration at 1.5 μM, 4.5 μM, and 15 μM. The signal intensity was presented in the bar chart below. Significant MRI signal was observed between the experimental group and the control group, where there were only apoptotic cells or avidin-GdDTPA or streptavidin-SPIO [77]. (Reprint with permission)

V-SPIO conjugates were tail vein injected to characterize the distribution within the tumor region. TUNEL assay of one tissue section from a slice of the tumor indicated the annexin V-SPIO conjugates were localized throughout the tumor region [78].

As one of the most widely applied imaging techniques in both clinical and research applications, MRI can provide useful information regarding cancer metabolic activity evaluation of treatment effects [79]. The hyperpolarized MRI (allows to measure the enzymatic conversion of administrated hyperpolarized molecules) [80] and chemical exchange saturation MRI (external compounds containing exchangeable protons that can be electively saturated and detected implicitly from water signal with better quality of sensitivity) [81] may lead to a future role for cancer treatment monitoring [55]. However, the inherently low sensitivity of MRI limits its application, which can only be remunerated by greater magnetic fields (4.7–14 T) with exogenous contrast agents and longer periods of data acquisition. Functional MRI including dynamic contrast-enhanced MRI (DCE-MRI) is one solution that has been used in the clinic for acquisition of serial MRI

images before, during, and after the administration of an MR contrast agent, allowing the visualization of contrast kinetic changes over long periods of time in addition to the bulk property of the tumor tissue. With the help of pharmacokinetic modeling, color-encoded images can be generated to characterize the tumor masses, identify stage, and even noninvasively monitor therapy [56]. Almost 100 clinical trials have utilized DCE-MRI to evaluate the therapeutic efficacy of antivascular agents [82]. Advanced techniques to enhance image processing, as well as multiparametric analysis, are needed to extend application of DCE-MRI and new purposeful imaging technologies in drug development for cancer therapy [82].

16.2.4 MRI for Detecting Other Markers of Treatment Response

With high spatiotemporal resolution, MRI can also be used to noninvasively detect gene expression in live animals. Mukherjee et al. report of using human water channel aquaporin1 as potential MRI reporters to produce MRI contrast. With 10% aquaporin-expression cells, the cell populations showed enhanced MRI signal. The researchers also explored the efficacy of using this system in a tumor xenograft model. With good contrast ability, biocompatibility, and engineering potential, aquaporin reporter genes could be remarkably applied to molecule imaging of MRI in cancer diagnosis and treatment monitoring.

16.3 Nuclear Imaging

Nuclear imaging is another type of a noninvasive imaging modality that utilizes radioactive isotopes to enable the imaging of biochemical components under normal and diseased conditions in living subjects. Based on the characteristics of the radiotracer, numerous aspects of biological processes can be aimed and visualized by using either PET or SPECT [83]. As discussed above, MRI plays an important role in visualizing the morphology of lesions and locating malignant sites. However, some biochemical processes inside a given tissue are difficult to detect with MRI due to the low sensitivity of the technique [84–86]. Therefore, PET and SPECT have become valuable techniques for monitoring the pharmacokinetics, biodistribution, and target site accumulation of nanomedicine formulations.

PET is an imaging technique that is used to visualize and quantify positron-emitting radionuclides [41], which facilitates four-dimensional (three spatial-dimensions plus temporal) quantitative measurements of the radioactive distribution within the human body in several medical fields including oncology [87]. The principle of dynamic detection by PET is based on annihilation, which occurs when the collision alters the mass of the positron and the electron into electromagnetic radiation after emitting a positron upon decay [83]. SPECT is similar to PET and

also utilizes radioactive isotopes. Nevertheless, SPECT isotopes emit a single photon upon decay, and detection of a single photon involves physical collimators, which shows low geometric competences to reject scattered photons as well as to adjust the vision field. Therefore, this technique is less sensitive than PET, limiting quantitative determinations of tracer accumulation [83, 88].

PET is widely applied to image tumor invasion and the interaction of tumor cells with stroma, including supporting proliferative signaling, avoiding growth suppression, and resisting cell death (apoptosis). The possibility of longitudinal assessment of specific biological processes rather than anatomic changes in tumor size increased the popularity of PET in recent years, providing insights into cellular metabolism for doctors, who are able to then direct further therapy plans for cancer patients. The previous section discussed some applications of MRI for imaging cellular activity, such as apoptosis. However, such markers serve as potential targets for enhancing contrast agent delivery rather than cellular activities that can be monitored by researchers. In contrast with nuclear imaging, monitoring of cellular activity, such as glucose metabolism, could be revolutionized with the use of isotope-labeled substrates [89]. The imaging of these specific types of cellular activity via PET was summarized in a recent review article [83]. For example, PET imaging utilizes ^{18}F, which is the most widely used radionuclide and has become an established clinical tool for whole-body imaging. Sgc8, which is a 41-oligonucleotide that targets protein tyrosine kinase-7 (PTK7), was labeled with F-18 via a two-step chemical synthesis. In the first step, ^{18}F-fluorobenzyl azide reacted with a spirocyclic hypervalent iodine(III) precursor via a one-step radiofluorination. The product was then conjugated with Sgc8-alkyne through copper-mediated “click” chemistry. The synthesized ^{18}F-Sgc8 was able to label aptamers (single-stranded DNA) robustly, allowing the quantification of PTK7 and colon carcinoma kinase-4 (CCK-4) [90]. PTK7 is upregulated in several human carcinomas and plays a major role in canonical Wnt signaling. The level of PTK7 strongly indicates the occurrence of colon carcinoma and thus is worth monitoring for diagnostic and prognostic purposes. An in vivo mouse xenograft study suggested that the 18-F radiolabeling methodology presented here is a powerful technique for tagging aptamers and chemical moieties with similar structures that are suitable for different targets. The quantification of PTK-7 using ^{18}F-Sgs 8 may be a potential strategy for cancer treatment monitoring [90] (Fig. 16.2).

16.3.1 Nuclear Imaging in Monitoring Tumor Growth

PET imaging has become a clinical keystone in cancer staging and restaging, serving as an important parameter in cancer therapeutic monitoring. The most frequently used PET contrast agent is [^{18}F]fluorodeoxyglucose (FDG), which is a glucose equivalent that is electively taken up by malignant cells with a high rate of glucose

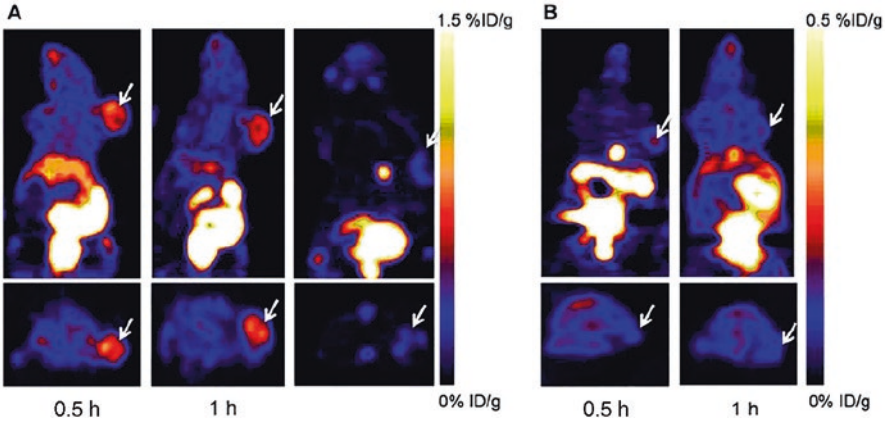

Fig. 16.2 Coronal (upper) and transaxial (lower) PET images of mice with HCT116 (**a**) and U87MG (**b**) xenograft injected with ^{18}F-Tr-Sgc8 at 30 min (0.5 h), 1 h (and 1 h co-injection with an excess amount of unlabeled aptamer (**a**, right panel) [90]. (Reprint with permission)

metabolism [91, 92]. FDG-PET imaging has been widely applied in staging multiple cancer types, including colorectal cancer, esophageal cancer, melanoma, head and neck cancer, non-small cell lung cancers, breast cancer, and lymphoma [91]. For example, FDG-PET was used to monitor patient treatment outcome after the first and third cycle of neoadjuvant chemotherapy in patients with late-stage ovarian cancer [93]. The results suggested sequential FDG-PET was capable of predicting patient therapeutic effects as early as immediately after the first cycle of neoadjuvant chemotherapy and was more accurate than traditional clinical or histopathological response criteria [93].

In addition to the tumor staging agent FDG, PET contrast agents for specifically monitoring the growth and death of tumor cells have also been reported. The essence of this strategy is to develop radiolabeled nucleoside equivalents like thymidine compounds that are able to incorporate into DNA, serving as convenient biomarkers of cell proliferation. Yaghoubi et al. reported PET imaging of thymidine kinase (herpes simplex virus type 1) or mutant HSV1-sr39tk reporter gene expression in mice and humans using 9-4-[^{18}F]fluoro-3-(hydroxymethyl)butyl]guanine ([^{18}F]FHBG) [94]. Another aspect of PET-based cell monitoring is the ability to utilize radiolabeled monoclonal antibodies specific for tumor-associated antigens, including Her2 and carcinoembryonic antigen. However, large protein-based contrast agents are slowly cleared from the blood stream and thus produce a high background signal [92]. Therefore, short-chain, engineered antibody fragments may enhance the signal by improving the signal-to-noise ratio, as they are vacant more speedily [91].

16.3.2 Nuclear Imaging in Monitoring Angiogenesis

As stated above, angiogenesis is a well-established marker for tumor growth, invasion, and metastasis [95]. Integrin $\alpha_v\beta_3$ represents an excellent molecular marker for angiogenesis, as it is significantly upregulated in activated endothelial cells in comparison to quiescent endothelial cells [96]. The Arg-Gly-Asp (RGD) tripeptide sequence is one of the most popular currently available integrin-targeted imaging probes because of its high affinity and specificity for integrin αvβ3 [97]. ^{18}F-Galacto-RGD was the first published RGD peptide conjugates in human subjects [98]. Upon that time, limited RGD containing PET probes have been designed and tested in the clinic. As their structures are different, all of the clinically studied RGD peptides, counting both monomers and dimers, exhibit very analogous in vivo pharmacokinetic properties [99]. The modification of the RGD sequence onto PET probes helps achieve multifunctional probes for accurate tumor metastasis monitoring. Zheng et al. assessed the diagnostic value of ^{68}Ga-NOTA-PRGD2 (NOTA-PEG$_4$-E[c(RGDfK)$_2$]) for PET/CT dual-modality imaging in 91 lung cancer patients (48 men and 43 women). The results of that study suggested an equal diagnostic efficacy for lung cancer but a better effect in assessing lymph node metastasis than ^{18}F-FDG [100] (Fig. 16.3).

16.3.3 Nuclear Imaging for Apoptosis

As stated in the previous section, strategies that enable the visualization and detection of apoptosis would have enormous benefits for treatment monitoring. Utilizing the interaction between Annexin V and PS is one of the most successful and widely applied strategies in apoptosis imaging [74]. This mechanism applies not only to MRI (previous section) but also to nuclear imaging and optical imaging (later section in this chapter). In 1998, Blankenberg et al. reported the preparation of ^{99m}Tc-hydrazinonicotinamide-Annexin V (^{99m}Tc-HYNIC-Annexin V). HYNIC is a nicotinic acid analogue with a bifunctional chelator that is capable of binding proteins on the one hand and sequestering ^{99m}Tc on the other. This molecule was conjugated to human rh-Annexin V and labeled with ^{99m}Tc using tricine as a co-ligand in the presence of stannous ions [101] (Fig. 16.4). A previous study demonstrated that the administered radiolabeled annexin V was able to locate and concentrate for apoptotic cells in vivo [101]. A two- to sixfold increase in the internalization of radiolabeled annexin V at sites of apoptosis was observed in the murine model of Fas-mediated apoptosis and treated murine lymphoma, suggesting that radiolabeled annexin V could be applicable for the detection and monitoring of tissues and organs undergoing programmed cell death [101]. In another study, Kartachova et al. reported the benefits of using ^{99m}Tc-HYNIC-annexin V assisting Pt(IV) chemotherapy in high-staged lung cancer. Significant correlation was observed between the monitoring of annexin V metabolic change via SPECT and the treatment outcome

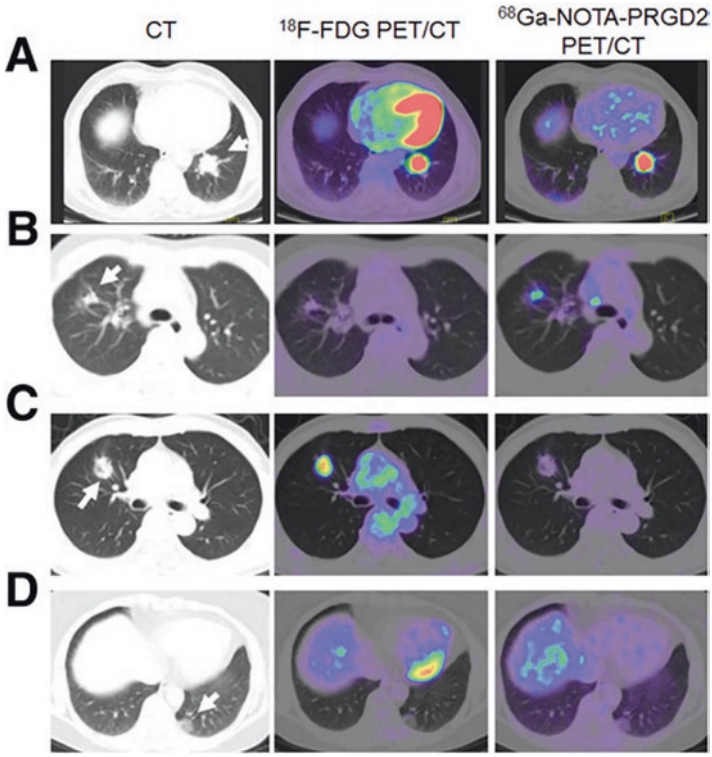

Fig. 16.3 CT, ^{18}F-FDG, and ^{68}Ga-NOTA-PRGD2 PET/CT images of primary lung cancer for four different patients (A, B, C, D). Patient A had an abstemiously differentiated adenocarcinoma in the inferior lobe of the left lung at the age of 76. Patients B and C were female with an exceedingly distinguished adenocarcinoma in the superior lobe of the right lung at the age of 37 and 61, respectively. Patient D was a 61-year-old woman with highly developed adenocarcinoma in the inferior lobe of the left lung. Patient A and B's lesions are strongly visualized on ^{68}Ga-NOTA-PRGD2 PET as the tumor sections show positive integrin $\alpha_v\beta_3$ staining. Arrows point to tumor [100]. (Reprint with permission)

from platinum chemotherapy, indicating ^{99m}Tc-HYNIC-annexin V is a promising therapeutic monitoring agent in human clinical application [102]. In addition to radiotracer ^{99m}Tc in nuclear medicine, many other radioligands are being used to image PS during apoptosis, as summarized in a published review [74].

In addition to radiolabeled protein probes, radiolabeled small-molecule probes are also available for apoptosis imaging via nuclear imaging. Compared with protein and peptide probes, small molecules have their own merits for clinical applications, including docile structural optimization and favorable pharmacokinetics such as organ distribution profiles, rapid diffusion rates, and blood clearance rates. Therefore, it is highly desirable to develop various small-molecule imaging probes with the same target binding affinity as proteins [74]. Zinc dipicolylamine (Zn-DPA) coordination complexes can be alternatives to Annexin V for PS targeting [103].

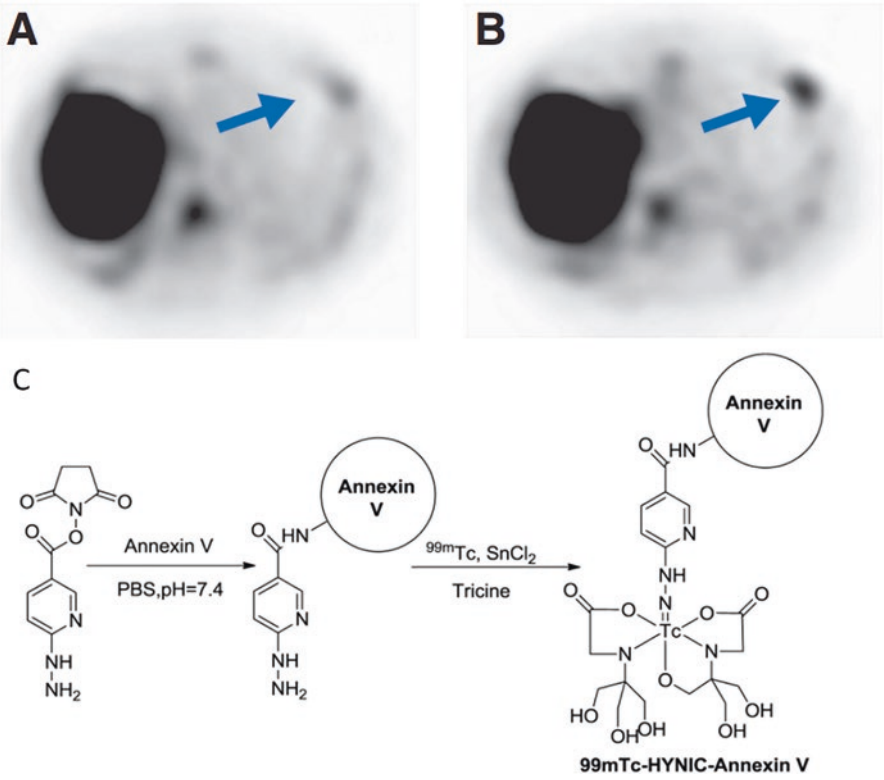

Fig. 16.4 The early ^{99m}Tc-HYNIC-annexin V tumor uptake could be a predictor of response to treatment in cancer patients [93], as demonstrated with a significant correlation between early therapy-induced changes in the probe tumor uptake and tumor response. SPECT images of tumor uptake in the rib region of metastasis before (**a**) and after (**b**) 48 h administration of cisplatin with ^{99m}Tc-HYNIC-annexin V [102]. (**c**) Radiochemistry of ^{99m}Tc-HYNIC-annexin V [74]. (Reprint with permission)

Zn^{2+} ions that mediate the cooperative association of the dipicolylamine ligand and the anionic head group of membrane-bound PS account for the targeting function of Zn-DPA [104]. Based on this information, to further develop this molecular strategy, Oltmanns et al. developed an ^{18}F-labeled zinc-cyclen probe that targets apoptosis [105]. With the ^{18}F label on zinc-cyclen, higher uptake was achieved in an exposed Dunning R3327-AT1 prostate tumor in comparison to the contralateral control tumor in PET imaging. This result suggests the great promise of this probe as a new agent for in vivo applications of treatment monitoring regarding cell death after different types of cancer therapy [105].

Radionuclide-based imaging techniques have been used routinely in clinics since the twenty-first century [55]. The use of molecular-targeted nanoparticles holds many benefits over conventional approaches to cancer treatment monitoring. First, a single nanoparticle can incorporate multiple imaging labels or combinations of

labels from different modalities, dramatically increasing the signal intensity. Second, nanoparticles with different chemical modification and conjugation target moieties are able to bypass biological barriers to improve the treatment monitoring efficacy [55]. Furthermore, recent advances in nuclear imaging systems provide high spatial and temporal resolution for treatment monitoring [106]. With the efforts of researchers in molecule imaging, we foresee the wide application of real-time monitoring with nuclear imaging to be a personalized patient-based treatment approach [107].

16.3.4 Nuclear Imaging for Detecting Other Markers of Treatment Response

Hormone receptors, such as estrogen receptors and progesterone receptors, have been identified as imaging targets in assisting breast cancer therapy staging and therapeutic monitoring. Therefore, many molecular imaging probes have been designed utilize this specific molecular cellular marker. Currin et al. reviewed current progress in predicting breast cancer endocrine responsiveness using 16-α[18F]-flouro-17β-estradiol PET (FES-PET). In general, estrogen-receptor imaging provides accurate measuring tumor response to endocrine therapy in patients [108]. Sun et al. also reported clinical evaluation of FES PEG/CT assisted in making personalized treatment decisions [109] for 33 breast cancer patients who underwent both 18F-FES and 18F-FDG PET/CT. With the three selected lung lesions, FES PET/CT showed one lesion with high update, and the other two lesions were negative, indicating an ER-positive metastasis or secondary primary tumor. Overall, 16 patients received adaptable treatment plans (different than original treatment plan) after FES PET/CT results [109]. These results indicated a good application of PET in assisting personalized adjustable treatment plans, beneficial for cancer treatment monitoring.

16.4 Optical Imaging

As a non-ionizing, noninvasive technique based on the precise optical characteristics of tissue components at different wavelengths, biomedical optical imaging has been developed to deliver quantitative measurements nearly in real time and with a wide range of resolutions, therefore providing high-quality images for the diagnosis and monitoring of treatment efficacy in cancer [110, 111]. However, there are limitations to the therapeutic monitoring of some treatments in patient responders and nonresponders. Researchers have been working to design reporter nanoparticles that can not only deliver chemotherapy or immunotherapy to the tumor but also report

back the efficacy in real time. Kulkarni et al. reported a reporter nanoparticle that monitors its efficacy in real time by presenting a dye activate/quench system inside the particle in addition to antitumor drug. If the experimental mice respond to the therapy, the activation of caspase-3 as part of the cellular apoptosis process will trigger the dye to show fluorescence. However, when the cells develop resistance to this treatment, no apoptosis or activation of caspase-3 will be available, leaving the quenched dye inside particles at the tumor site [112].

Fluorescence reflectance imaging (FRI) is by far the most extensively used optical imaging technique [41]. The ease, versatility, and sensitivity of optical imaging make it possible to image multiple fluorophores in the same animal, which is the most significant benefit of this technique. Kumar et al. reported a mitochondrial-targeting antitumor drug that consists of both 5′-deoxy-5-fluorouridine and apoptotic marker ethidium. By targeting the elevated expression level of H_2O_2 inside mitochondria, 5′-deoxy-5-fluorouridine and ethidium will be released. By monitoring the intrinsic fluorescence changes of ethidium, therapeutic effect would be monitored both in vitro and in vivo [113].

Recent studies focused on addressing the drawbacks of optical imaging, including autofluorescence, poor penetration depth, and limited anatomical information [41]. For example, nanomaterials labeled with fluorescent dyes often tend to use longer wavelengths for excitation (e.g., Alexa Fluor 647, Cy5, or Cy7), which are outside the range of natural autofluorescence [114]. On the other hand, some in vivo studies have validated the potency of quantum dots accumulation in cancer region for optical imaging to enhance the tissue penetration depth [115]. The fluorescent nanoparticles that are currently being used in noninvasive imaging include organic dye-doped nanoparticles, quantum dots, and upconversion nanoparticles. The emergent development of innovative multifunctional nanoparticles can easily be combined with therapeutics to form nanotheranostic materials. For example, NIR dye Cy5.5-labeled chitosan nanoparticles with encapsulated paclitaxel were able to image and assess therapeutic efficacy in mice with SCC7 murine squamous carcinoma tumors [116]. In addition to encapsulating chemotherapeutics, optical imaging-guided photodynamic therapy is a widely exploited technique for cancer treatment [13]. Through the activation of the administered tumor-localizing photosensitizing agents by particulate wavelength photons, the surrounding tumor tissues can be irreversibly photodamaged after a series of biological processes [117]. Luo et al. reported the synthesis of a mitochondria-targeted near-infrared (NIR) photosensitizer for simultaneous cancer photodynamic therapy (PDT) and photothermal therapy. The small-molecule photosensitizer was designed utilizing many synthesized heptamethine cyanine dyes that are able to concentrate in cancer cells via organic-anion transporting polypeptide-mediated active delivery and are retained in mitochondria due to their cationic properties. Furthermore, these photosensitizers for NIR imaging can distinguish the tumor margins from healthy tissue, serving as excellent candidates for precise imaging-guided phototherapy and treatment monitoring [118].

16.4.1 Optical Imaging in Monitoring Angiogenesis

As stated in the previous section, VEGF plays an important role in angiogenesis activity. Here we use one specific example to discuss the use of potential dye-conjugated anti-VEGF to obtain quantitative information about VEGFR expression. Wang et al. developed an Avidin-tagged $VEGF_{121}$ protein, which could form a stable complex with streptavidin-IRDye800 (SA800) after being biotinylated with the bacterial BirA biotin ligase. The dye-associated complex is capable of interacting with VEGFR in vitro at high affinity. In addition, the complex also displayed efficacy for receptor-specific targeting in a 67NR mice xenograft model [119]. Figure 16.6 presents the in vivo imaging of 67NR tumors with IRDye800 conjugates. The $VEGF_{121}$-Avid/SA800 complex may be a potential clinical tool for quantitative and repetitive NIR imaging of VEGFR expression for monitoring cancer treatment (Fig. 16.5) [119].

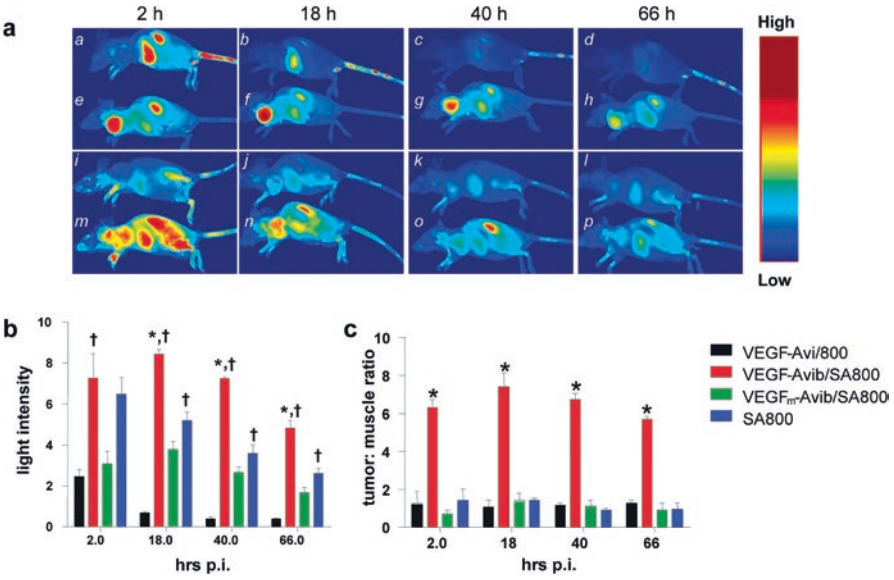

Fig. 16.5 In vivo NIR imaging of 67NR tumor models with IRDye800 conjugates. (**a**) Sagittal images were taken at 2, 18, 40, and 66 h after administration of chemically modified VEGF121-Avi-IRDye800 (VEGF-Avi/800) intravenously (a–d), VEGF121-Avi-biotin/streptavidin-IRDye800 (VEGF-Avib/SA800) (e–h), VEGF mutant-Avi-biotin/streptavidin-IRDye800 (VEGFm-Avib/SA800) (i–l), and streptavidin-IRDye800 (SA800) (m–p). Total fluorescence signals were acquired under the same conditions and normalized by exposure time and ROI area (total signal/ms mm^2). (**b**) Light intensity of tumor and (**c**) tumor to muscle light intensity proportion at multiple time points were presented as bar graphs after administration of certain type of dye complexes [119]. (Reprint with permission)

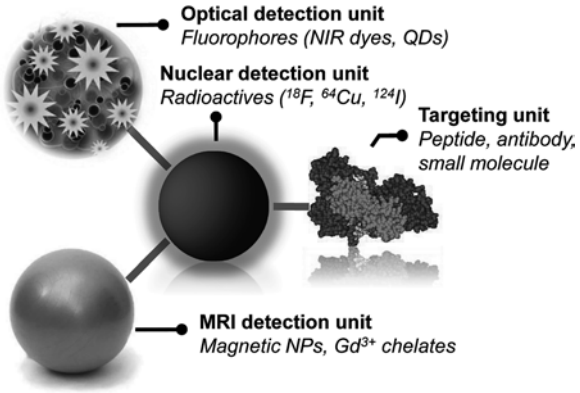

Fig. 16.6 Schematic diagram of multimodality imaging probes. Radioactive isotopes, magnetic particles, fluorophores, and targeting motifs can be integrated into one single system with different combinations. *NIR* near-infrared, *NP* nanoparticles, *QD* quantum dot [120]. (Reprint with permission)

16.4.2 Optical Imaging in Monitoring Apoptosis

In the field of optical imaging, researchers are attempting to monitor apoptosis via advanced probes. The design of optical imaging probes for apoptosis usually falls into two strategies. The first strategy is to conjugate a fluorophore on the probes as a reporter signal. Similar to the strategy described above, utilizing the annexin V-PS binding mechanism, researchers attempted to label annexin-V with the near-infrared fluorophore Cy5.5 [121]. As expected, the conjugation preserves the binding affinity to PS. However, when more than 2 dyes are conjugated, annexin no longer binds to PS [74]. To overcome these limitations, Ntziachristos et al. demonstrated that tumor responses to chemotherapy can be resolved accurately via fluorescence tomography with PS fluorescent probe based on a Cy 5.5 modified annexin V (two types of modification were performed with annexin C. The ratio of Cy 5.5 to annexin V was either 1.1 or 2.4) [122]. A tenfold increase in the fluorescent signal in cyclophosphamide-sensitive tumors and a sevenfold increase in resistant tumors were observed for monitoring apoptosis [122].

The other strategy is to design fluorophore-quenching probes. These activatable probes do not emit a signal continuously and thus allow researchers to control and manipulate the outputs of maximized target signal and minimized background signal by altering the chemical environments. Lee et al. reported an apoptosis nanoprobe that is able to deliver chemically tagged, dual-quenching caspase-3-sensitive fluorogenic peptides into cells, allowing caspase-3-dependent fluorescence intensification to be imaged real-time in apoptotic cells with high resolution [123]. The self-assembled hyaluronic acid nanoparticles were conjugated with a caspase-3-specific substrate to detect apoptosis in cells. The NIR fluorescence quencher BHQ3 and the dye Cy5.5 was conjugated onto hyaluronic acid particle. When interacting with apoptotic cells, the active caspase-3 in apoptotic cells will cleave the bond that connects BHQ3 and Cy 5.5. When Cy 5.5 is cut free from the particle, it would induce strong fluorescent signal of the cells. The system is shown to

effectively identify not only for apoptotic cells in vitro but also in vivo tumor tissue in mice treated after DOX [123].

In contrast to the fluorophore-quenching strategy, aggregation-induced emission properties have also been designed for monitoring drug-induced apoptosis inside single cell. Yuan et al. reported a chemotherapeutic Pt(IV) prodrug with the conjugation of cyclic-RGD peptide as well as caspase-3 enzyme peptide (Asp-Glu-Val-Asp, DEVD) conjugated tetraphenylsilole (TPS) fluorophore (TPS-DEVD). While TPS-DEVD is non-florescent under normal aqueous condition, TPS residue after dissociation with DEVD tends to aggregate to emit fluorescent. The cleavage of DEVD process is controlled by caspase-3, which only happens in response to apoptotic cells. The smart design of nanomaterial could be potentially used as molecular imaging probes for early cancer therapeutic evaluation.

16.4.3 Intraoperative Positioning

In addition to traditional optical imaging examination for cancer diagnosis and prognosis, surgery also plays a key role in cancer treatment. In fact, tumor dissection is the initial treatment for most benign tumors and many malignant tumors. The inherent difficulties in distinguishing tumor and normal tissue make it difficult to perform the procedure. Intraoperative positioning is defined as fluorescent labeling routine that utilizes an imaging system to enable surgeons to distinguish between healthy and malignant tissues that are labeled with a fluorescent detection agent [124]. Despite the wide application of CT, MRI, PET, and SPECT for preoperative tumor diagnosis, such techniques are typically not applicable for intraoperative tumor surgery, and palpation and graphic inspection remain the leading approaches [124, 125]. On the other hand, fluorescence molecular imaging (FMI) has been well known as a dominant tool for guiding accurate intraoperative positioning [126–129]. To facilitate more discriminating tumor detection, fluorescent dyes can be modified with targeting moieties (i.e., peptides, antibodies, or sugars) that are processed systemically and accumulate at lesion sites. Still in the preclinical stage, such fluorescent imaging probes show potential as markers for cancer cells and tumor angiogenesis, making them a desirable surgical guide for imaging tumor microenvironments (Table 16.1), although some of these probes may require a long time for FDA approval [124].

Over the past decade, this technology has enhanced the ability to surgically remove liver metastases[128], breast cancer[129], ovarian cancer[130], melanoma[131], vulvar cancer[132] and cervical cancer[133]. Recently, Kircher et al. reported the use of a gliosarcoma model to explore functional nanoparticles as intraoperative optical probes[134]. Such nanoparticles can be synthesized simply with a strong NIRF signal, enabling real-time imaging for surgical procedures. The intracellular infiltration, extended degradation, and combined optical and magnetic properties of nanoparticles allow radiologists and neurosurgeons to identify the same probe in the same cells, augmenting the precision of surgical resection and the

Table 16.1 Examples of ongoing optical probe clinical trials

Name	Sponsor	Phase	Patient population	ClinicalTrials.gov Identifier	Function
RACPP AVB-620	Avelas Biosciences, Inc.	I	Women with primary, nonrecurrent breast cancer undergoing surgery	NCT02391194	Surgical margins; sentinel lymph node biopsy
LUM105	David Kirsch Lumicell, Inc.	I	Patients with the following conditions: sarcoma, soft tissue sarcoma, breast cancer, colorectal cancer, pancreatic cancer, esophageal cancer	NCT01626066, NCT02438358, NCT02584244	Surgical margins
Tumor Paint (BLZ-100)	Blaze Bioscience Australia Pty Ltd, Blaze Bioscience Inc.,	I	Patients with the following conditions: skin neoplasms, soft tissue sarcoma, central nervous system tumors, glioma, breast cancer	NCT02097875, NCT02464332, NCT02462629, NCT02234297, NCT02496065	Surgical margins
OTL38	On Target Laboratories, LLC	II	Intraoperative imaging of folate receptor α-positive ovarian cancer	NCT02317705	Surgical margins

outlook for many brain cancer patients[134]. Similarly, they also developed nanoparticles containing a gold core with Raman-active layer and a silicone coating with Gd-DOTA to precisely identify the margins of brain tumors in living mice both preoperatively and intraoperatively. The nanoparticles injected intravenously accumulated at the tumor cite whereas none was found in the surrounding healthy tissue, indicating the potential in brain tumor imaging and resection[135].

16.5 Multimodality Imaging for Cancer Treatment Monitoring

In the design of novel clinical diagnostic probes, several parameters are generally considered, including detection sensitivity, spatial resolution, tissue penetration, temporal resolution, signal-to-noise ratio, and quantitative accuracy [136]. Therefore, the design and utilization of multiple modalities simultaneously have become popular in clinical research to overcome the limitations of single imaging techniques [137]. Since the first PET/CT multimodal instrument was introduced in 1997, the sales of monomodal, PET imaging equipment have gradually declined [138–140]. In 2007, the first commercial PET/MRI hybrid prototype human-size

scanner was released, triggering tremendous research in probe design for such dual-imaging techniques [141]. Considering the continuing development of multimodal instrumentation, researchers are currently focused on tracking several molecular targets simultaneously or using different imaging approaches in combination to more precisely identify the localization and expression of certain biochemical markers [141, 142]. A single probe with multimodal detectability is not necessary when designing imaging probes but could help guarantee the same pharmacokinetics and localization of signal from each modality, reducing the stress on the body's blood clearance system. Due to the different sensitivity of each imaging modality (may vary by three orders of magnitude), the concentrations of contrast agents of each modality within a single probe must be carefully considered to meet the requirements for imaging while remaining nontoxic to the human body [137]. Lee et al. summarized the design of multimodality probes for molecular imaging (Fig. 16.6) [120].

An example of an imaging probe for nuclear and MRI combinations was reported by Lee et al. [143]. Polyaspartic acid-coated iron oxide nanoparticles with superficial amino groups were conjugated to cyclic-RGD peptides for integrin $\alpha_v\beta_3$ targeting and macrocyclic 1, 4, 7, 10-tetraazacyclododecane-N, N′, N″, N‴-tetraacetic acid (DOTA) chelators for PET after labeling with ^{64}Cu. The modified iron oxide nanoparticles were further evaluated in vitro and in vivo to demonstrate the efficacy and feasibility of receptor targeting for dual PET/MRI (Fig. 16.7) [143].

In another case, amine-functionalized quantum dots (QD) were modified with RGD peptides and DOTA chelators for integrin $\alpha_v\beta_3$-targeted PET/NIRF imaging

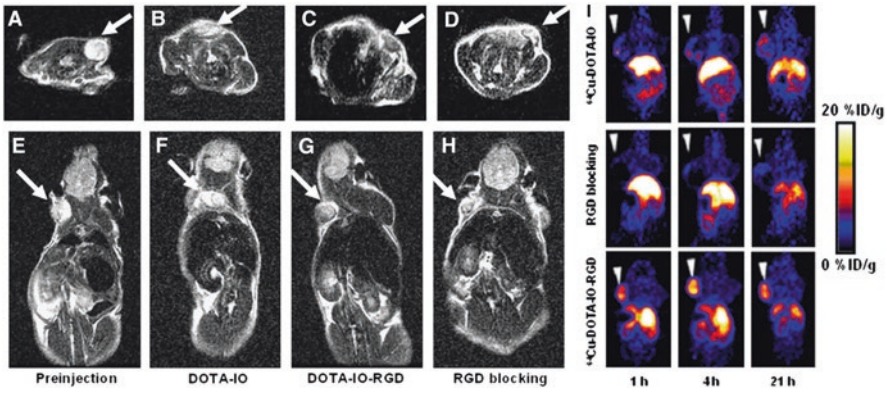

Fig. 16.7 (**a**–**h**) T_2-weighted MR images of mice with U87MG tumor before injection of unmodified iron oxide nanoparticles (**a** and **e**) and at 4 h after tail-vein injection of DOTA-labeled iron oxide nanoparticles (**b** and **f**), DOTA−/RGD-labeled iron oxide nanoparticles (**c** and **g**), and DOTA−/RGD-labeled iron oxide nanoparticle with blocking dose of c(RGDyK) (**d** and **h**). (**i**) Entire body coronal PET images of mouse with human U87MG xenograft at 1, 4, and 21 h after injection of 3.7 MBq of ^{64}Cu-/DOTA-labeled iron oxide nanoparticles, ^{64}Cu-/DOTA−/RGD-labeled iron oxide nanoparticles, or ^{64}Cu-/DOTA−/RGD-labeled iron oxide nanoparticles with c(RGDyK) peptide per kilogram (300 mg of iron equivalent iron oxide nanoparticles per mouse) [143]. (Reprint with permission)

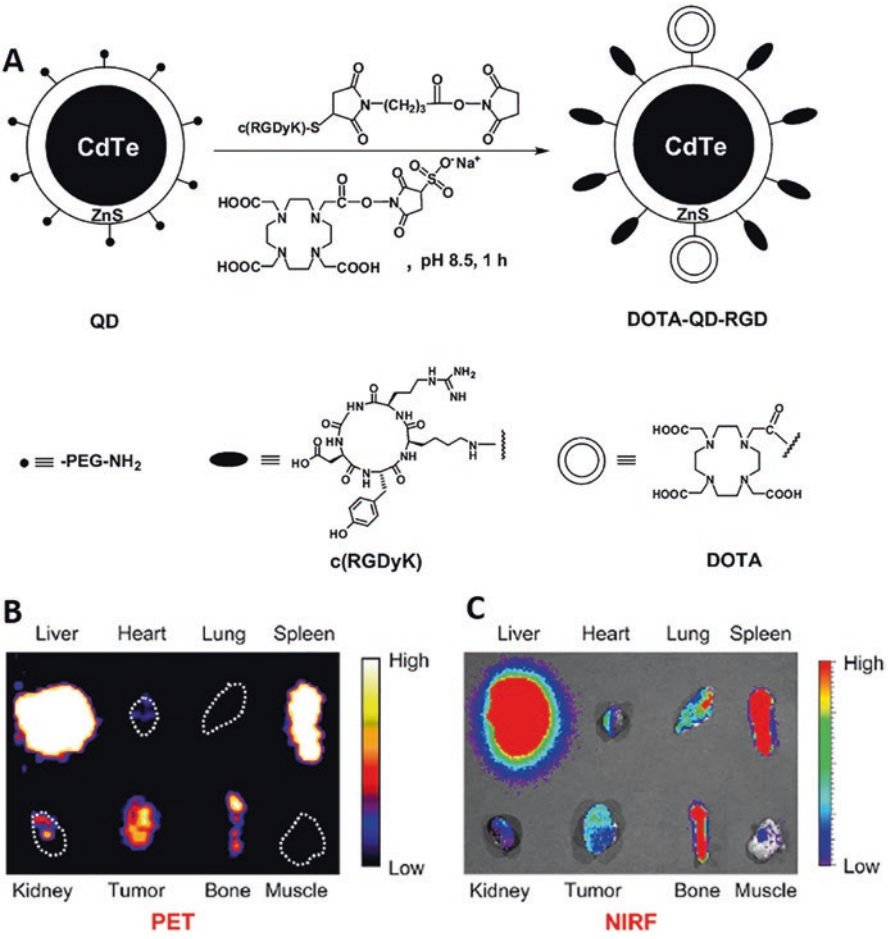

Fig. 16.8 (**a**) Synthesis of dual-function PET/NIRF probe DOTA–QD–RGD. (**b**) PET and (**c**) NIRF image of harvested tissues 5 h after administration of 64Cu-labeled DOTA–QD–RGD [144]

[144]. PET/NIRF imaging, tissue homogenate fluorescence measurements, and immunofluorescence staining were performed with human glioblastoma tumor xenograft-bearing mice to determine the probe uptake amount at the malignancy site and in the major organs (Fig. 16.8) [144]. The liver and spleen exhibited the highest signal intensity for both PET and NIRF. However, the signal at the tumor site was enhanced in comparison to other organs. Cornell dots (C dots) are another categorized optical dye for cancer therapy [145]. The Bradbury group reported the first-in-human clinical trial of using ^{124}I-cRGDY-PEG-C dots in patients with metastatic melanoma. ^{124}I-cRGDY-PEG-C dots were intravenously introduced into patients followed by serial PET and CT assessment to identify the safety pharmacokinetics, clearance profiles, and radiation dosimetry. No adverse effects were observed in metabolic profiles with conventional tests of blood and urine samples

from the patients injected with ^{124}I-cRGDY-PEG-C dots during a 2-week period, indicating the safety of using this PET/optical dual probe for melanoma diagnosis [145].

An easy strategy for designing an optical/MRI dual-functional probe is to fuse MRI contrast agents with QDs through a doping procedure. While doping into bulk semiconductors with transition metals is routine, doping into nanocrystals has been demanding owing to the small size and confined structure. Researchers have attempted to dope manganese into different QDs, such as ZeS [146], ZnS [147], CdSe [148], and InP [146]. In addition, ZnO QDs have also been doped with a number of other transition metals, including Ti, Cr, Co, Ni, Mn, Ru, Pd, Fe, and Ag. However, considering the toxicity of such heavy metals, the clinical applications of transition metal doped QDs are not feasible [137, 149]. In 2012, Bourlinos et al. described Gd(III)-doped carbon dots served as fluorescence-MRI probes for theranostic applications [150]. The obtained Gd(III)-doped carbon dots stably disperse in water, with a size of 3–4 nm in diameter and an even gadolinium distribution on the surface. An ex vivo study suggested that these dots exhibit strong T_1-weighted MRI contrast, bright fluorescence, and low cytotoxicity [150].

Multimodal imaging probes have been designed to visualize apoptosis in vitro and in vivo. In 2004, Schellenberger et al. reported the synthesis of a magneto/optical form of annexin V via the conjugation of Cy5.5 and annexin to an amino-CLIO (cross-linked iron oxide) nanoparticle. The conjugation process preserves the strength of the interaction between annexin V and apoptotic Jurkat T cells while making it possible to detect the particles by using either MRI or NIRF optical methods [105]. Small-molecule multimodal probes are also available, such as the molecular probe LS498, which consists of DOTA for chelating the radionuclide ^{64}Cu, an NIR fluorophore-quencher pair and caspase-3-specific peptide substrates, which is able to trace cellular apoptosis via PET and optical imaging both in vitro and in vivo.

Recently, photoacoustic imaging has gained popularity in the field of multimodal imaging, which has the potential to image animal and human organs with both high-contrast and good spatial resolution [151]. The photoacoustic consequence is the physical basis for photoacoustic imaging and denotes to the creation of acoustic waves by the absorption of electromagnetic energy, including optical or radio-frequency waves [152]. With the current introduction of targeted contrast agents, photoacoustics is capable of molecular imaging in vivo, thus expediting further molecular cellular characterization of cancer in the context of both diagnostic and therapeutic monitoring [153]. Photoacoustic imaging enables the visualization of tumor locations deep within a tissue and provides information about the vasculature [154]. This approach is also able to offer details about hemoglobin oxygen saturation at high resolution with high contrast, without the use of exogenous contrast agents [155], which is superior to other imaging techniques such as blood oxygen level-dependent-MRI and PET [153]. Wang et al. reported the synthesis of ferritin (Fn) nanocages with ultrasmall copper sulfide (CuS) nanoparticles inside the nanocage cavities using a biomimetic synthetic approach. The biological function of Fn is to remove superfluous iron ions in body fluids and accumulate inside its own interior cavity, making it good iron bank as our photoacoustics imaging probes. CuS–Fn

nanocages (CuS–Fn NCs) showed robust near-infrared absorbance and extraordinary photothermal conversion efficiency. Following the guidance of PAI and PET, photothermal therapy with CuS–Fn NCs exhibited great cancer therapeutic efficiency with low toxicity effect both in vitro and in vivo, demonstrating the great potential of bioinspired novel CuS–Fn NCs as clinically translatable cancer theranostics while monitoring tumor/tumor vasculature shrinkage simultaneously. This highly sensitive, noninvasive, and quantitative in vivo guidance method may be suitable for cancer theranostics in applications such as cancer diagnosis, treatment, or drug delivery [156]. Though recent studies are still at the preclinical research stage, movement toward clinical trials is expected for these novel and intricately designed multimodality imaging probes [120]. In another example, Nie et al. reported of synthesizing plasmonic gold nanostars conjugated with cyclic-RGD peptides (RGD-GNS) for photoacoustic imaging to target tumor vasculature environment with elevated $\alpha_v\beta_3$ expression. After injection of the RGD-GNS, tumor-associated blood vessels were clearly visualized, and tumor size was significantly shrink after photoacoustic application [151].

16.6 Conclusion and Challenges

The development of nanotheranostics principles and techniques requires a multidisciplinary approach (including chemistry, physics, material science, drug delivery, and pharmacology) to work toward the common goal of improving the management of cancer. As stated earlier in this chapter, the synchronized delivery of imaging agents and therapeutics will provide the possibility of early diagnosis and feedback on treatment efficacy in real time without the need for traditional endpoints.

However, despite the enthusiasm concerning the use of sophisticated nanotheranostics for cancer applications, many improvements are needed before nanotheranostics can become an effective therapy in clinical practice. Many of the techniques discussed above have only been evaluated in vitro and may not prove to be feasible as imaging and theranostic agents in vivo. Some of the nanotheranostic agents have been investigated in vivo; however, such studies focused on imaging functionality, while the therapeutic effectiveness was largely unknown. Nevertheless, for those nanotheranostics whose imaging and therapeutic efficacy have been investigated, the path for clinical translation is still challenging and strewn with impediments. Drug/imaging agent loading capability, biocompatibility, pharmacokinetic/pharmacodynamics parameters, and risk/advantage estimation must to be investigated. It is worth noting that the dose for nanotheranostics may be different than the dose needed for single therapeutics or imaging probes because the simultaneous therapeutic and diagnostic effect may be altered by several orders of magnitude compared to the effect of a single probe [13, 157]. Additionally, there is a great need for better predictors (biomarkers) of therapeutic response that can be monitored using imaging via nanoparticles early in the treatment cycle, such as hormone receptors discussed in the previous study. Recently, the development of tumor-derived extra-

cellular vesicles could also be used to identify cancer biomarkers, such as ephrin type-A receptor 2 in pancreatic cancer [158]. With further specific biomarkers identified, biomedical engineers can utilize engineering techniques to refine assays for clinical use. Furthermore, multiple in vivo studies and clinical trials would be needed in collaboration with clinicians. Ultimately, the key considerations in the design of an effective therapeutic and an effective imaging agent will be (1) the good biocompatibility and controlled clearance rate for better therapeutic monitoring, (2) the identification and understanding of cancer biomarkers and how molecular imaging agents interact with the biomarkers, (3) the rational design of materials to target cancer tissue environment to better serve the purpose of molecular engineering, and (4) the capability to manufacture the materials in large scale under sterile condition for clinical application [159, 160].

The successful use of noninvasive imaging techniques will improve cancer diagnosis and therapeutic effects. As each of the modalities discussed above has its own advantages and disadvantages, dual- or multimodality theranostic will demonstrate their benefits and synergy in the context of the need to accurately and quantitatively resolve biomedical questions [41]. Ultimately, in theory, theranostic agents can deliver therapeutics to tumors and can use imaging functions to improve the application of diagnosis and therapeutic monitoring.

Acknowledgments This work was supported by the College of Engineering and Mathematics, University of Vermont; MOST of China (Grant Nos. 2017YFA0205201, 2014CB744503, and 2013CB733802); the NSFC under Grant Nos. 81422023, 81371596, 51273165, U1705281, and U1505221; the Program for New Century Excellent Talents in University (NCET-13-0502); the Fundamental Research Funds for the Central Universities, China (20720150206 and 20720150141); and the Intramural Research Program, National Institute of Biomedical Imaging and Bioengineering, National Institutes of Health.

References

1. Siegel, R.L., Miller, K.D., Jemal, A.: Cancer statistics, 2017. CA Cancer J. Clin. **67**(1), 7–30 (2017). https://doi.org/10.3322/caac.21387
2. Smith, R.A., Andrews, K.S., Brooks, D., Fedewa, S.A., Manassaram-Baptiste, D., Saslow, D., Brawley, O.W., Wender, R.C.: Cancer screening in the United States, 2017: a review of current American Cancer Society guidelines and current issues in cancer screening. CA Cancer J. Clin. **67**(2), 100–121 (2017). https://doi.org/10.3322/caac.21392
3. Lim, Z.-Z.J., Li, J.-E.J., Ng, C.-T., Yung, L.-Y.L., Bay, B.-H.: Gold nanoparticles in cancer therapy. Acta Pharmacol. Sin. **32**(8), 983–990 (2011)
4. Walker, N.F., Gan, C., Olsburgh, J., Khan, M.S.: Diagnosis and management of intradiverticular bladder tumours. Nat. Rev. Urol. **11**(7), 383–390 (2014). https://doi.org/10.1038/nrurol.2014.131
5. Carbone, A., Vaccher, E., Gloghini, A., Pantanowitz, L., Abayomi, A., de Paoli, P., Franceschi, S.: Diagnosis and management of lymphomas and other cancers in HIV-infected patients. Nat. Rev. Clin. Oncol. **11**(4), 223–238 (2014). https://doi.org/10.1038/nrclinonc.2014.31
6. Liu, Z., Chen, X.: Simple bioconjugate chemistry serves great clinical advances: albumin as a versatile platform for diagnosis and precision therapy. Chem. Soc. Rev. (2016)

7. Choi, K.Y., Liu, G., Lee, S., Chen, X.: Theranostic nanoplatforms for simultaneous cancer imaging and therapy: current approaches and future perspectives. Nanoscale. **4**(2), 330–342 (2012). https://doi.org/10.1039/c1nr11277e
8. Wang, J., Mi, P., Lin, G., Wáng, Y.X.J., Liu, G., Chen, X.: Imaging guided delivery of RNAi for anticancer treatment. Adv. Drug Deliv. Rev. (2016)
9. Miao, T., Rao, K.S., Spees, J.L., Floreani, R.A.: Osteogenic differentiation of human mesenchymal stem cells through alginate-graft-poly(ethylene glycol) microsphere-mediated intracellular growth factor delivery. J. Control. Release. **192**, 57–66 (2014). https://doi.org/10.1016/j.jconrel.2014.06.029
10. Miao, T., Fenn, S.L., Charron, P.N., Floreani, R.A.: Self-healing and thermoresponsive dual-cross-linked alginate hydrogels based on supramolecular inclusion complexes. Biomacromolecules. **16**(12), 3740–3750 (2015). https://doi.org/10.1021/acs.biomac.5b00940
11. Miao, T., Miller, E.J., McKenzie, C., Floreani, R.A.: Physically crosslinked polyvinyl alcohol and gelatin interpenetrating polymer network theta-gels for cartilage regeneration. J. Mater. Chem. B. **3**(48), 9242–9249 (2015). https://doi.org/10.1039/C5TB00989H
12. O'Brien, F.J.: Biomaterials & scaffolds for tissue engineering. Mater. Today. **14**(3), 88–95 (2011). https://doi.org/10.1016/S1369-7021(11)70058-X
13. Mura, S., Couvreur, P.: Nanotheranostics for personalized medicine. Adv. Drug Deliv. Rev. **64**(13), 1394–1416 (2012). https://doi.org/10.1016/j.addr.2012.06.006
14. Liu, Y., Miyoshi, H., Nakamura, M.: Nanomedicine for drug delivery and imaging: a promising avenue for cancer therapy and diagnosis using targeted functional nanoparticles. Int. J. Cancer. **120**(12), 2527–2537 (2007). https://doi.org/10.1002/ijc.22709
15. Chi, X., Huang, D., Zhao, Z., Zhou, Z., Yin, Z., Gao, J.: Nanoprobes for in vitro diagnostics of cancer and infectious diseases. Biomaterials. **33**(1), 189–206 (2012). https://doi.org/10.1016/j.biomaterials.2011.09.032
16. Pirmohamed, M., Ferner, R.E.: Monitoring drug treatment. BMJ. **327**(7425), 1179–1181 (2003)
17. Weissleder, R., Mahmood, U.: Molecular imaging. Radiology. **219**(2), 316–333 (2001). https://doi.org/10.1148/radiology.219.2.r01ma19316
18. Bao, G., Mitragotri, S., Tong, S.: Multifunctional nanoparticles for drug delivery and molecular imaging. Annu. Rev. Biomed. Eng. **15**, 253–282 (2013). https://doi.org/10.1146/annurev-bioeng-071812-152409
19. Cleary, K., Peters, T.M.: Image-guided interventions: technology review and clinical applications. Annu. Rev. Biomed. Eng. **12**, 119–142 (2010). https://doi.org/10.1146/annurev-bioeng-070909-105249
20. Bhattarai, N., Bhattarai, S.R.: Theranostic nanoparticles: a recent breakthrough in nanotechnology. J. Nanomed. Nanotechnol. **2012**, (2012)
21. Mody, V.V., Siwale, R., Singh, A., Mody, H.R.: Introduction to metallic nanoparticles. J. Pharm Bioall Sci. **2**(4), 282–289 (2010). https://doi.org/10.4103/0975-7406.72127
22. Corr, S.A.: Metal oxide nanoparticles. In: Nanoscience: Volume 1: Nanostructures through Chemistry, vol. 1, pp. 180–207. The Royal Society of Chemistry, London, UK (2013). https://doi.org/10.1039/9781849734844-00180
23. Bangal, M., Ashtaputre, S., Marathe, S., Ethiraj, A., Hebalkar, N., Gosavi, S.W., Urban, J., Kulkarni, S.K.: Semiconductor nanoparticles. Hyperfine Interact. **160**(1), 81–94 (2005). https://doi.org/10.1007/s10751-005-9151-y
24. Liberman, A., Mendez, N., Trogler, W.C., Kummel, A.C.: Synthesis and surface functionalization of silica nanoparticles for nanomedicine. Surf. Sci. Rep. **69**(2-3), 132–158 (2014). https://doi.org/10.1016/j.surfrep.2014.07.001
25. Dinarvand, R., Sepehri, N., Manoochehri, S., Rouhani, H., Atyabi, F.: Polylactide-co-glycolide nanoparticles for controlled delivery of anticancer agents. Int. J. Nanomedicine. **6**, 877–895 (2011). https://doi.org/10.2147/IJN.S18905
26. Guilherme, M.R., Mauricio, M.R., Tenório-Neto, E.T., Kunita, M.H., Cardozo-Filho, L., Cellet, T.S.P., Pereira, G.M., Muniz, E.C., da Rocha, S.R.P., Rubira, A.F.: Polycaprolactone

nanoparticles containing encapsulated progesterone prepared using a scCO2 emulsion drying technique. Mater. Lett. **124**, 197–200 (2014). https://doi.org/10.1016/j.matlet.2014.03.099
27. Langer, K., Anhorn, M.G., Steinhauser, I., Dreis, S., Celebi, D., Schrickel, N., Faust, S., Vogel, V.: Human serum albumin (HSA) nanoparticles: reproducibility of preparation process and kinetics of enzymatic degradation. Int. J. Pharm. **347**(1–2), 109–117 (2008). https://doi.org/10.1016/j.ijpharm.2007.06.028
28. Cardoso, V.S., Quelemes, P.V., Amorin, A., Primo, F.L., Gobo, G.G., Tedesco, A.C., Mafud, A.C., Mascarenhas, Y.P., Corrêa, J.R., Kuckelhaus, S.A., Eiras, C., Leite, J.R.S., Silva, D., dos Santos Júnior, J.R.: Collagen-based silver nanoparticles for biological applications: synthesis and characterization. J. Nanobiotechnol. **12**(1), 36 (2014). https://doi.org/10.1186/s12951-014-0036-6
29. Wicki, A., Witzigmann, D., Balasubramanian, V., Huwyler, J.: Nanomedicine in cancer therapy: challenges, opportunities, and clinical applications. J. Control. Release. **200**, 138–157 (2015). https://doi.org/10.1016/j.jconrel.2014.12.030
30. Duncan, R., Gaspar, R.: Nanomedicine(s) under the microscope. Mol. Pharm. **8**(6), 2101–2141 (2011). https://doi.org/10.1021/mp200394t
31. Brindle, K.: New approaches for imaging tumour responses to treatment. Nat. Rev. Cancer. **8**(2), 94–107 (2008)
32. National Lung Screening Trial Research T: The National Lung Screening Trial: overview and study design. Radiology. **258**(1), 243–253 (2011). https://doi.org/10.1148/radiol.10091808
33. Irion, K.L., Hochhegger, B., Marchiori, E., Porto, N.S., Baldisserotto, S.V., Santana, P.R.: Radiograma de tórax e tomografia computadorizada na avaliação do enfisema pulmonar. J. Bras. Pneumol. **33**, 720–732 (2007)
34. McLaughlin, R., Hylton, N.: MRI in breast cancer therapy monitoring. NMR Biomed. **24**(6), 712–720 (2011). https://doi.org/10.1002/nbm.1739
35. Avril, N.E., Weber, W.A.: Monitoring response to treatment in patients utilizing PET. Radiol. Clin. N. Am. **43**(1), 189–204 (2005)
36. Cai, J., Li, F.: Single-photon emission computed tomography tracers for predicting and monitoring cancer therapy. Curr. Pharm. Biotechnol. **14**(7), 693–707 (2013)
37. Falou, O., Sadeghi-Naini, A., Soliman, H., Yaffe, M.J., Czarnota, G.J.: Diffuse optical imaging for monitoring treatment response in breast cancer patients. Conf. Proc IEEE Eng. Med. Biol. Soc. **2012**, 3155–3158 (2012). https://doi.org/10.1109/embc.2012.6346634
38. Hrkach, J., Von Hoff, D., Ali, M.M., Andrianova, E., Auer, J., Campbell, T., De Witt, D., Figa, M., Figueiredo, M., Horhota, A., Low, S., McDonnell, K., Peeke, E., Retnarajan, B., Sabnis, A., Schnipper, E., Song, J.J., Song, Y.H., Summa, J., Tompsett, D., Troiano, G., Van Geen Hoven, T., Wright, J., LoRusso, P., Kantoff, P.W., Bander, N.H., Sweeney, C., Farokhzad, O.C., Langer, R., Zale, S.: Preclinical development and clinical translation of a PSMA-targeted Docetaxel nanoparticle with a differentiated pharmacological profile. Sci. Transl. Med. **4**(128), 128ra139-128ra139 (2012). https://doi.org/10.1126/scitranslmed.3003651
39. Janib, S.M., Moses, A.S., MacKay, J.A.: Imaging and drug delivery using theranostic nanoparticles. Adv. Drug Deliv. Rev. **62**(11), 1052–1063 (2010). https://doi.org/10.1016/j.addr.2010.08.004
40. Villaraza, A.J.L., Bumb, A., Brechbiel, M.W.: Macromolecules, Dendrimers and Nanomaterials in magnetic resonance imaging: the interplay between size, function and pharmacokinetics. Chem. Rev. **110**(5), 2921–2959 (2010). https://doi.org/10.1021/cr900232t
41. Kunjachan, S., Ehling, J., Storm, G., Kiessling, F., Lammers, T.: Noninvasive imaging of Nanomedicines and Nanotheranostics: principles, Progress, and prospects. Chem. Rev. (2015). https://doi.org/10.1021/cr500314d
42. Miao, T., Zhang, Y., Zeng, Y., Tian, R., Liu, G.: Functional nanoparticles for molecular imaging-guided gene delivery and therapy. In: Dai, Z. (ed.) Advances in Nanotheranostics II: Cancer Theranostic Nanomedicine, pp. 273–305. Springer Singapore, Singapore (2016). https://doi.org/10.1007/978-981-10-0063-8_8

43. Lu, J., Feng, F., Jin, Z.: Cancer diagnosis and treatment guidance: role of MRI and MRI probes in the era of molecular imaging. Curr. Pharm. Biotechnol. **14**(8), 714–722 (2013)
44. Strijkers, G.J., Mulder, W.J., van Tilborg, G.A., Nicolay, K.: MRI contrast agents: current status and future perspectives. Anti Cancer Agents Med. Chem. **7**(3), 291–305 (2007)
45. Su, H., Wu, C., Zhu, J., Miao, T., Wang, D., Xia, C., Zhao, X., Gong, Q., Song, B., Ai, H.: Rigid Mn(II) chelate as efficient MRI contrast agent for vascular imaging. Dalton Trans. **41**(48), 14480–14483 (2012). https://doi.org/10.1039/c2dt31696j
46. Luo, K., Tian, J., Liu, G., Sun, J., Xia, C., Tang, H., Lin, L., Miao, T., Zhao, X., Gao, F., Gong, Q., Song, B., Shuai, X., Ai, H., Gu, Z.: Self-assembly of SiO2/Gd-DTPA-polyethylenimine nanocomposites as magnetic resonance imaging probes. J. Nanosci. Nanotechnol. **10**(1), 540–548 (2010)
47. Phillips, W.T., Bao, A., Sou, K., Li, S., Goins, B.: Radiolabeled liposomes as drug delivery nanotheranostics. In: Drug Delivery Applications of Noninvasive Imaging, pp. 252–267. John Wiley & Sons, Inc, Hoboken, NJ, USA (2013). https://doi.org/10.1002/9781118356845.ch11
48. Luk, B.T., Fang, R.H., Zhang, L.: Lipid- and polymer-based nanostructures for cancer theranostics. Theranostics. **2**(12), 1117–1126 (2012). https://doi.org/10.7150/thno.4381
49. Kaida, S., Cabral, H., Kumagai, M., Kishimura, A., Terada, Y., Sekino, M., Aoki, I., Nishiyama, N., Tani, T., Kataoka, K.: Visible drug delivery by supramolecular nanocarriers directing to single-platformed diagnosis and therapy of pancreatic tumor model. Cancer Res. **70**(18), 7031–7041 (2010). https://doi.org/10.1158/0008-5472.can-10-0303
50. Yu, M.K., Jeong, Y.Y., Park, J., Park, S., Kim, J.W., Min, J.J., Kim, K., Jon, S.: Drug-loaded superparamagnetic iron oxide nanoparticles for combined cancer imaging and therapy in vivo. Angew. Chem. Int. Ed. Engl. **47**(29), 5362–5365 (2008). https://doi.org/10.1002/anie.200800857
51. Ng, T.S., Wert, D., Sohi, H., Procissi, D., Colcher, D., Raubitschek, A.A., Jacobs, R.E.: Serial diffusion MRI to monitor and model treatment response of the targeted nanotherapy CRLX101. Clin. Cancer Res. **19**(9), 2518–2527 (2013). https://doi.org/10.1158/1078-0432.ccr-12-2738
52. Folkman, J.: Tumor angiogenesis: therapeutic implications. N. Engl. J. Med. **285**(21), 1182–1186 (1971). https://doi.org/10.1056/nejm197111182852108
53. Bergers, G., Hanahan, D.: Modes of resistance to anti-angiogenic therapy. Nat. Rev. Cancer. **8**(8), 592–603 (2008). https://doi.org/10.1038/nrc2442
54. Wang, Z., Dabrosin, C., Yin, X., Fuster, M.M., Arreola, A., Rathmell, W.K., Generali, D., Nagaraju, G.P., El-Rayes, B., Ribatti, D., Chen, Y.C., Honoki, K., Fujii, H., Georgakilas, A.G., Nowsheen, S., Amedei, A., Niccolai, E., Amin, A., Ashraf, S.S., Helferich, B., Yang, X., Guha, G., Bhakta, D., Ciriolo, M.R., Aquilano, K., Chen, S., Halicka, D., Mohammed, S.I., Azmi, A.S., Bilsland, A., Keith, W.N., Jensen, L.D.: Broad targeting of angiogenesis for cancer prevention and therapy. Semin. Cancer Biol. **35**, Supplement:S224–Supplement:S243 (2015). https://doi.org/10.1016/j.semcancer.2015.01.001
55. Cai, W., Chen, X.: Multimodality molecular imaging of tumor angiogenesis. J. Nucl. Med. **49**(Suppl 2), 113S–128S (2008). https://doi.org/10.2967/jnumed.107.045922
56. Choyke, P.L., Dwyer, A.J., Knopp, M.V.: Functional tumor imaging with dynamic contrast-enhanced magnetic resonance imaging. J. Magn. Reson. Imaging. **17**(5), 509–520 (2003). https://doi.org/10.1002/jmri.10304
57. O'Connor, J.P.B., Jackson, A., Parker, G.J.M., Jayson, G.C.: DCE-MRI biomarkers in the clinical evaluation of antiangiogenic and vascular disrupting agents. Br. J. Cancer. **96**(2), 189–195 (2007). https://doi.org/10.1038/sj.bjc.6603515
58. Knopp, M.V., Weiss, E., Sinn, H.P., Mattern, J., Junkermann, H., Radeleff, J., Magener, A., Brix, G., Delorme, S., Zuna, I., van Kaick, G.: Pathophysiologic basis of contrast enhancement in breast tumors. J. Magn. Reson. Imaging. **10**(3), 260–266 (1999)
59. Wang, B., Gao, Z.Q., Yan, X.: Correlative study of angiogenesis and dynamic contrast-enhanced magnetic resonance imaging features of hepatocellular carcinoma. Acta. Radiol. **46**(4), 353–358 (2005)

60. Korpanty, G., Carbon, J.G., Grayburn, P.A., Fleming, J.B., Brekken, R.A.: Monitoring response to anticancer therapy by targeting microbubbles to tumor vasculature. Clin. Cancer Res. **13**(1), 323–330 (2007). https://doi.org/10.1158/1078-0432.ccr-06-1313
61. Campbell, I.D., Humphries, M.J.: Integrin structure, activation, and interactions. Cold Spring Harb. Perspect. Biol. **3**(3), (2011). https://doi.org/10.1101/cshperspect.a004994
62. Danhier, F., Le Breton, A., Preat, V.: RGD-based strategies to target alpha(v) beta(3) integrin in cancer therapy and diagnosis. Mol. Pharm. **9**(11), 2961–2973 (2012). https://doi.org/10.1021/mp3002733
63. Tan, M., Lu, Z.-R.: Integrin targeted MR imaging. Theranostics. **1**, 83–101 (2011)
64. Sipkins, D.A., Cheresh, D.A., Kazemi, M.R., Nevin, L.M., Bednarski, M.D., Li, K.C.: Detection of tumor angiogenesis in vivo by alphaVbeta3-targeted magnetic resonance imaging. Nat. Med. **4**(5), 623–626 (1998)
65. Barrett, T., Brechbiel, M., Bernardo, M., Choyke, P.L.: MRI of tumor angiogenesis. J. Magn. Reson. Imaging. **26**(2), 235–249 (2007). https://doi.org/10.1002/jmri.20991
66. Lecouvet, F.E., Talbot, J.N., Messiou, C., Bourguet, P., Liu, Y., de Souza, N.M.: Monitoring the response of bone metastases to treatment with Magnetic Resonance Imaging and nuclear medicine techniques: a review and position statement by the European Organisation for Research and Treatment of Cancer imaging group. Eur. J. Cancer. **50**(15), 2519–2531 (2014). https://doi.org/10.1016/j.ejca.2014.07.002
67. Heyn, C., Ronald, J.A., Ramadan, S.S., Snir, J.A., Barry, A.M., MacKenzie, L.T., Mikulis, D.J., Palmieri, D., Bronder, J.L., Steeg, P.S., Yoneda, T., MacDonald, I.C., Chambers, A.F., Rutt, B.K., Foster, P.J.: In vivo MRI of cancer cell fate at the single-cell level in a mouse model of breast cancer metastasis to the brain. Magn. Reson. Med. **56**(5), 1001–1010 (2006). https://doi.org/10.1002/mrm.21029
68. Steichen, S.D., Caldorera-Moore, M., Peppas, N.A.: A review of current nanoparticle and targeting moieties for the delivery of cancer therapeutics. Eur J. Pharm. Sci. **48**(3), 416–427 (2013). https://doi.org/10.1016/j.ejps.2012.12.006
69. Elmore, S.: Apoptosis: a review of programmed cell death. Toxicol. Pathol. **35**(4), 495–516 (2007). https://doi.org/10.1080/01926230701320337
70. Balcer-Kubiczek, E.K.: Apoptosis in radiation therapy: a double-edged sword. Exp. Oncol. **34**(3), 277–285 (2012)
71. Kaufmann, S.H., Earnshaw, W.C.: Induction of apoptosis by cancer chemotherapy. Exp. Cell Res. **256**(1), 42–49 (2000). https://doi.org/10.1006/excr.2000.4838
72. Mouratidis, P.X., Rivens, I., Ter Haar, G.: A study of thermal dose-induced autophagy, apoptosis and necroptosis in colon cancer cells. Int. J. Hyperthermia. **31**(5), 476–488 (2015). https://doi.org/10.3109/02656736.2015.1029995
73. Panzarini, E., Tenuzzo, B., Dini, L.: Photodynamic therapy-induced apoptosis of HeLa cells. Ann. N. Y. Acad. Sci. **1171**, 617–626 (2009). https://doi.org/10.1111/j.1749-6632.2009.04908.x
74. Zeng, W., Wang, X., Xu, P., Liu, G., Eden, H.S., Chen, X.: Molecular imaging of apoptosis: from micro to macro. Theranostics. **5**(6), 559–582 (2015). https://doi.org/10.7150/thno.11548
75. Marino, G., Kroemer, G.: Mechanisms of apoptotic phosphatidylserine exposure. Cell Res. **23**(11), 1247–1248 (2013). https://doi.org/10.1038/cr.2013.115
76. Blanco, V.M., Latif, T., Chu, Z., Qi, X.: Imaging and therapy of pancreatic cancer with phosphatidylserine-targeted nanovesicles. Transl. Oncol. **8**(3), 196–203 (2015). https://doi.org/10.1016/j.tranon.2015.03.011
77. Jung, H.-i., Kettunen, M.I., Davletov, B., Brindle, K.M.: Detection of apoptosis using the C2A domain of synaptotagmin I. Bioconjug. Chem. **15**(5), 983–987 (2004). https://doi.org/10.1021/bc049899q
78. Zhao, M., Beauregard, D.A., Loizou, L., Davletov, B., Brindle, K.M.: Non-invasive detection of apoptosis using magnetic resonance imaging and a targeted contrast agent. Nat. Med. **7**(11), 1241–1244 (2001)

79. García-Figueiras, R., Padhani, A.R., Baleato-González, S.: Therapy monitoring with functional and molecular MR imaging. Magn. Reson. Imaging Clin. N. Am. **24**(1), 261–288 (2016). https://doi.org/10.1016/j.mric.2015.08.003
80. Schroeder, M.A., Clarke, K., Neubauer, S., Tyler, D.J.: Hyperpolarized magnetic resonance: a novel technique for the in vivo assessment of cardiovascular disease. Circulation. **124**(14), 1580–1594 (2011). https://doi.org/10.1161/circulationaha.111.024919
81. van Zijl, P.C.M., Yadav, N.N.: Chemical exchange saturation transfer (CEST): what is in a name and what isn't? Magn. Reson. Med. **65**(4), 927–948 (2011). https://doi.org/10.1002/mrm.22761
82. O'Connor, J.P., Jackson, A., Parker, G.J., Roberts, C., Jayson, G.C.: Dynamic contrast-enhanced MRI in clinical trials of antivascular therapies. Nat. Rev. Clin. Oncol. **9**(3), 167–177 (2012). https://doi.org/10.1038/nrclinonc.2012.2 http://www.nature.com/nrclinonc/journal/v9/n3/suppinfo/nrclinonc.2012.2_S1.html
83. Jacobson, O., Chen, X.: Interrogating tumor metabolism and tumor microenvironments using molecular positron emission tomography imaging. Theranostic approaches to improve therapeutics. Pharmacol. Rev. **65**(4), 1214–1256 (2013). https://doi.org/10.1124/pr.113.007625
84. Nishimura, K., Hida, S., Nishio, Y., Ohishi, K., Okada, Y., Okada, K., Yoshida, O., Nishimura, K., Nishibuchi, S.: The validity of magnetic resonance imaging (MRI) in the staging of bladder cancer: comparison with computed tomography (CT) and transurethral ultrasonography (US). Jpn. J. Clin. Oncol. **18**(3), 217–226 (1988)
85. Ryu, J.S., Kim, J.S., Moon, D.H., Kim, S.M., Shin, M.J., Chang, J.S., Park, S.K., Han, D.J., Lee, H.K.: Bone SPECT is more sensitive than MRI in the detection of early osteonecrosis of the femoral head after renal transplantation. J. Nucl. Med. **43**(8), 1006–1011 (2002)
86. Spanaki, M.V., Spencer, S.S., Corsi, M., MacMullan, J., Seibyl, J., Zubal, I.G.: Sensitivity and specificity of quantitative difference SPECT analysis in seizure localization. J. Nucl. Med. **40**(5), 730–736 (1999)
87. Wang, J., Maurer, L.: Positron emission tomography: applications in drug discovery and drug development. Curr. Top. Med. Chem. **5**(11), 1053–1075 (2005)
88. Rahmim, A., Zaidi, H.: PET versus SPECT: strengths, limitations and challenges. Nucl. Med. Commun. **29**(3), 193–207 (2008). https://doi.org/10.1097/MNM.0b013e3282f3a515
89. Malviya, G., Nayak, T.K.: PET imaging to monitor cancer therapy. Curr. Pharm. Biotechnol. **14**(7), 669–682 (2013)
90. Jacobson, O., Weiss, I., Wang, L., Wang, Z., Yang, X., Dewhurst, A., Ma, Y., Zhu, G., Niu, G., Kiesewetter, D.O., Vasdev, N., Liang, S., Chen, X.: 18F-labeled single-stranded DNA aA. for PET imaging of protein tyrosine Kinase-7 expression. J. Nucl. Med. (2015). https://doi.org/10.2967/jnumed.115.160960
91. Weissleder, R.: Molecular imaging in cancer. Science (New York, N.Y.). **312**(5777), 1168–1171 (2006). https://doi.org/10.1126/science.1125949
92. Quon, A., Gambhir, S.S.: FDG-PET and beyond: molecular breast cancer imaging. J. Clin Oncol. **23**(8), 1664–1673 (2005). https://doi.org/10.1200/jco.2005.11.024
93. Avril, N., Sassen, S., Schmalfeldt, B., Naehrig, J., Rutke, S., Weber, W.A., Werner, M., Graeff, H., Schwaiger, M., Kuhn, W.: Prediction of response to neoadjuvant chemotherapy by sequential F-18-fluorodeoxyglucose positron emission tomography in patients with advanced-stage ovarian cancer. J. Clin Oncol. **23**(30), 7445–7453 (2005). https://doi.org/10.1200/jco.2005.06.965
94. Yaghoubi, S.S., Gambhir, S.S.: PET imaging of herpes simplex virus type 1 thymidine kinase (HSV1-tk) or mutant HSV1-sr39tk reporter gene expression in mice and humans using [18F] FHBG. Nat. Protocols. **1**(6), 3069–3074 (2007). http://www.nature.com/nprot/journal/v1/n6/suppinfo/nprot.2006.459_S1.html
95. Folkman, J.: Role of angiogenesis in tumor growth and metastasis. Semin. Oncol. **29**(6 Suppl 16), 15–18 (2002). https://doi.org/10.1053/sonc.2002.37263
96. Weis, S.M., Cheresh, D.A.: αv integrins in angiogenesis and cancer. Cold Spring Harb. Perspect. Med. **1**(1), a006478 (2011). https://doi.org/10.1101/cshperspect.a006478

97. Humphries, J.D., Byron, A., Humphries, M.J.: Integrin ligands at a glance. J. Cell Sci. **119**(19), 3901–3903 (2006). https://doi.org/10.1242/jcs.03098
98. Haubner, R., Kuhnast, B., Mang, C., Weber, W.A., Kessler, H., Wester, H.J., Schwaiger, M.: [18F]Galacto-RGD: synthesis, radiolabeling, metabolic stability, and radiation dose estimates. Bioconjug. Chem. **15**(1), 61–69 (2004). https://doi.org/10.1021/bc034170n
99. Niu, G., Chen, X.: RGD PET: from lesion detection to therapy response monitoring. J. Nucl. Med. (2015). https://doi.org/10.2967/jnumed.115.168278
100. Zheng, K., Liang, N., Zhang, J., Lang, L., Zhang, W., Li, S., Zhao, J., Niu, G., Li, F., Zhu, Z., Chen, X.: 68Ga-NOTA-PRGD2 PET/CT for integrin imaging in patients with lung cancer. J. Nucl. Med. **56**(12), 1823–1827 (2015). https://doi.org/10.2967/jnumed.115.160648
101. Blankenberg, F.G., Katsikis, P.D., Tait, J.F., Davis, R.E., Naumovski, L., Ohtsuki, K., Kopiwoda, S., Abrams, M.J., Darkes, M., Robbins, R.C.: In vivo detection and imaging of phosphatidylserine expression during programmed cell death. Proc. Natl. Acad. Sci. **95**(11), 6349–6354 (1998)
102. Kartachova, M., van Zandwijk, N., Burgers, S., van Tinteren, H., Verheij, M., Valdes Olmos, R.A.: Prognostic significance of 99mTc Hynic-rh-annexin V scintigraphy during platinum-based chemotherapy in advanced lung cancer. J. Clin. Oncol. **25**(18), 2534–2539 (2007). https://doi.org/10.1200/jco.2006.10.1337
103. Koulov, A.V., Stucker, K.A., Lakshmi, C., Robinson, J.P., Smith, B.D.: Detection of apoptotic cells using a synthetic fluorescent sensor for membrane surfaces that contain phosphatidylserine. Cell Death Differ. **10**(12), 1357–1359 (2003). https://doi.org/10.1038/sj.cdd.4401315
104. Kwong, J.M.K., Hoang, C., Dukes, R.T., Yee, R.W., Gray, B.D., Pak, K.Y., Caprioli, J.: Bis(Zinc-Dipicolylamine), Zn-DPA, a new marker for apoptosis. Invest. Ophthalmol. Vis. Sci. **55**(8), 4913–4921 (2014). https://doi.org/10.1167/iovs.13-13346
105. Oltmanns, D., Zitzmann-Kolbe, S., Mueller, A., Bauder-Wuest, U., Schaefer, M., Eder, M., Haberkorn, U., Eisenhut, M.: Zn(II)-bis(cyclen) complexes and the imaging of apoptosis/necrosis. Bioconjug. Chem. **22**(12), 2611–2624 (2011). https://doi.org/10.1021/bc200457b
106. Khalil, M.M., Tremoleda, J.L., Bayomy, T.B., Gsell, W.: Molecular SPECT imaging: an overview. Int. J. Molecul. Imag. **2011**, (2011). https://doi.org/10.1155/2011/796025
107. Thorwarth, D.: Radiotherapy treatment planning based on functional PET/CT imaging data. Nucl. Med. Rev. **15**(C), 43–47 (2012)
108. Currin, E., Linden, H.M., Mankoff, D.A.: Predicting breast Cancer endocrine responsiveness using molecular imaging. Curr. Breast Cancer Rep. **3**(4), 205–211 (2011). https://doi.org/10.1007/s12609-011-0053-5
109. Sun, Y., Yang, Z., Zhang, Y., Xue, J., Wang, M., Shi, W., Zhu, B., Hu, S., Yao, Z., Pan, H., Zhang, Y.: The preliminary study of 16α-[18F]fluoroestradiol PET/CT in assisting the individualized treatment decisions of breast Cancer patients. PLoS One. **10**(1), e0116341 (2015). https://doi.org/10.1371/journal.pone.0116341
110. Costas, B.: Review of biomedical optical imaging—a powerful, non-invasive, non-ionizing technology for improving in vivo diagnosis. Meas. Sci. Technol. **20**(10), 104020 (2009)
111. Weissleder, R., Ntziachristos, V.: Shedding light onto live molecular targets. Nat. Med. **9**(1), 123–128 (2003)
112. Kulkarni, A., Rao, P., Natarajan, S., Goldman, A., Sabbisetti, V.S., Khater, Y., Korimerla, N., Chandrasekar, V., Mashelkar, R.A., Sengupta, S.: Reporter nanoparticle that monitors its anticancer efficacy in real time. Proc. Natl. Acad. Sci. **113**(15), E2104–E2113 (2016). https://doi.org/10.1073/pnas.1603455113
113. Kumar, R., Han, J., Lim, H.-J., Ren, W.X., Lim, J.-Y., Kim, J.-H., Kim, J.S.: Mitochondrial induced and self-monitored intrinsic apoptosis by antitumor Theranostic Prodrug: in vivo imaging and precise Cancer treatment. J. Am. Chem. Soc. **136**(51), 17836–17843 (2014). https://doi.org/10.1021/ja510421q

114. Buchwalow, I.B., Böcker, W.: Antibodies for immunohistochemistry. In: Immunohistochemistry: Basics and Methods, pp. 1–8. Springer, New York City, NY, USA (2010)
115. Nune, S.K., Gunda, P., Thallapally, P.K., Lin, Y.-Y., Forrest, M.L., Berkland, C.J.: Nanoparticles for biomedical imaging. Expert Opin. Drug Deliv. **6**(11), 1175–1194 (2009). https://doi.org/10.1517/17425240903229031
116. Kim, K., Kim, J.H., Park, H., Kim, Y.S., Park, K., Nam, H., Lee, S., Park, J.H., Park, R.W., Kim, I.S., Choi, K., Kim, S.Y., Park, K., Kwon, I.C.: Tumor-homing multifunctional nanoparticles for cancer theragnosis: simultaneous diagnosis, drug delivery, and therapeutic monitoring. J. Control. Release. **146**(2), 219–227 (2010). https://doi.org/10.1016/j.jconrel.2010.04.004
117. Allison, R.R.: Photodynamic therapy: oncologic horizons. Future Oncol. **10**(1), 123–124 (2014). https://doi.org/10.2217/fon.13.176
118. Luo, S., Tan, X., Fang, S., Wang, Y., Liu, T., Wang, X., Yuan, Y., Sun, H., Qi, Q., Shi, C.: Mitochondria-targeted small-molecule fluorophores for dual modal Cancer phototherapy. Adv. Funct. Mater. **26**(17), 2826–2835 (2016). https://doi.org/10.1002/adfm.201600159
119. Wang, H., Chen, K., Niu, G., Chen, X.: Site-specifically biotinylated VEGF121 for near-infrared fluorescence imaging of tumor angiogenesis. Mol. Pharm. **6**(1), 285–294 (2009). https://doi.org/10.1021/mp800185h
120. Lee, S., Chen, X.: Dual-modality probes for in vivo molecular imaging. Mol. Imaging. **8**(2), 87–100 (2009)
121. Petrovsky, A., Schellenberger, E., Josephson, L., Weissleder, R., Bogdanov Jr., A.: Near-infrared fluorescent imaging of tumor apoptosis. Cancer Res. **63**(8), 1936–1942 (2003)
122. Ntziachristos, V., Schellenberger, E.A., Ripoll, J., Yessayan, D., Graves, E., Bogdanov, A., Josephson, L., Weissleder, R.: Visualization of antitumor treatment by means of fluorescence molecular tomography with an annexin V–Cy5.5 conjugate. Proc. Natl. Acad. Sci. U. S. A. **101**(33), 12294–12299 (2004). https://doi.org/10.1073/pnas.0401137101
123. Lee, S., Choi, K.Y., Chung, H., Ryu, J.H., Lee, A., Koo, H., Youn, I.-C., Park, J.H., Kim, I.-S., Kim, S.Y., Chen, X., Jeong, S.Y., Kwon, I.C., Kim, K., Choi, K.: Real time, high resolution video imaging of apoptosis in single cells with a polymeric nanoprobe. Bioconjug. Chem. **22**(2), 125–131 (2011). https://doi.org/10.1021/bc1004119
124. Chi, C., Du, Y., Ye, J., Kou, D., Qiu, J., Wang, J., Tian, J., Chen, X.: Intraoperative imaging-guided cancer surgery: from current fluorescence molecular imaging methods to future multi-modality imaging technology. Theranostics. **4**(11), 1072–1084 (2014). https://doi.org/10.7150/thno.9899
125. Vahrmeijer, A.L., Hutteman, M., van der Vorst, J.R., van de Velde, C.J.H., Frangioni, J.V.: Image-guided cancer surgery using near-infrared fluorescence. Nat. Rev. Clin. Oncol. **10**(9), 507–518 (2013). https://doi.org/10.1038/nrclinonc.2013.123
126. Nguyen, Q.T., Tsien, R.Y.: Fluorescence-guided surgery with live molecular navigation [mdash] a new cutting edge. Nat. Rev. Cancer. **13**(9), 653–662 (2013). https://doi.org/10.1038/nrc3566
127. van Dam, G.M., Themelis, G., Crane, L.M.A., Harlaar, N.J., Pleijhuis, R.G., Kelder, W., Sarantopoulos, A., de Jong, J.S., Arts, H.J.G., van der Zee, A.G.J., Bart, J., Low, P.S., Ntziachristos, V.: Intraoperative tumor-specific fluorescence imaging in ovarian cancer by folate receptor-[alpha] targeting: first in-human results. Nat. Med. **17**(10), 1315–1319 (2011). http://www.nature.com/nm/journal/v17/n10/abs/nm.2472.html#supplementary-information
128. van der Vorst, J.R., Schaafsma, B.E., Hutteman, M., Verbeek, F.P., Liefers, G.J., Hartgrink, H.H., Smit, V.T., Lowik, C.W., van de Velde, C.J., Frangioni, J.V., Vahrmeijer, A.L.: Near-infrared fluorescence-guided resection of colorectal liver metastases. Cancer. **119**(18), 3411–3418 (2013). https://doi.org/10.1002/cncr.28203
129. Sugie, T., Sawada, T., Tagaya, N., Kinoshita, T., Yamagami, K., Suwa, H., Ikeda, T., Yoshimura, K., Niimi, M., Shimizu, A., Toi, M.: Comparison of the indocyanine green fluorescence and blue dye methods in detection of sentinel lymph nodes in early-stage breast cancer. Ann. Surg. Oncol. **20**(7), 2213–2218 (2013). https://doi.org/10.1245/s10434-013-2890-0

130. Kim, H.S., Ahn, J.H., Chung, H.H., Kim, J.W., Park, N.H., Song, Y.S., Lee, H.P., Kim, Y.B.: Impact of intraoperative rupture of the ovarian capsule on prognosis in patients with early-stage epithelial ovarian cancer: a meta-analysis. Eur. J. Surg. Oncol. **39**(3), 279–289 (2013). https://doi.org/10.1016/j.ejso.2012.12.003
131. Azarpira, N., Asadi, N., Torabineghad, S., Taghipour, M.: Metastatic malignant melanoma intraoperative imprint cytology of brain tumor. J. Cytol. **29**(3), 192–193 (2012). https://doi.org/10.4103/0970-9371.101170
132. Crane, L.M., Themelis, G., Arts, H.J., Buddingh, K.T., Brouwers, A.H., Ntziachristos, V., van Dam, G.M., van der Zee, A.G.: Intraoperative near-infrared fluorescence imaging for sentinel lymph node detection in vulvar cancer: first clinical results. Gynecol. Oncol. **120**(2), 291–295 (2011). https://doi.org/10.1016/j.ygyno.2010.10.009
133. Baldauf, J., Muller, J.U., Fleck, S., Hinz, P., Chiriac, A., Schroeder, H.W.: The value of intraoperative three dimensional fluoroscopy in anterior decompressive surgery of the cervical spine. Zentralbl. Neurochir. **69**(1), 30–34 (2008). https://doi.org/10.1055/s-2007-992796
134. Kircher, M.F., Mahmood, U., King, R.S., Weissleder, R., Josephson, L.: A multimodal nanoparticle for preoperative magnetic resonance imaging and intraoperative optical brain tumor delineation. Cancer Res. **63**(23), 8122–8125 (2003)
135. Kircher, M.F., de la Zerda, A., Jokerst, J.V., Zavaleta, C.L., Kempen, P.J., Mittra, E., Pitter, K., Huang, R., Campos, C., Habte, F., Sinclair, R., Brennan, C.W., Mellinghoff, I.K., Holland, E.C., Gambhir, S.S.: A brain tumor molecular imaging strategy using a new triple-modality MRI-photoacoustic-Raman nanoparticle. Nat. Med. **18**(5), 829–834 (2012). http://www.nature.com/nm/journal/v18/n5/abs/nm.2721.html#supplementary-information
136. Cherry, S.R.: Multimodality in vivo imaging systems: twice the power or double the trouble? Annu. Rev. Biomed. Eng. **8**(1), 35–62 (2006). https://doi.org/10.1146/annurev.bioeng.8.061505.095728
137. Louie, A.: Multimodality imaging probes: design and challenges. Chem. Rev. **110**(5), 3146–3195 (2010). https://doi.org/10.1021/cr9003538
138. Pomper, M.G., Gelovani, J.G.: Molecular Imaging in Oncology. Informa Health Care, New York (2008)
139. Ell, P.J.: The contribution of PET/CT to improved patient management. Br. J. Radiol. **79**(937), 32–36 (2006). https://doi.org/10.1259/bjr/18454286
140. Tsukamoto, E., Ochi, S.: PET/CT today: system and its impact on cancer diagnosis. Ann. Nucl. Med. **20**(4), 255–267 (2006)
141. Cherry, S.R., Louie, A.Y., Jacobs, R.E.: The integration of positron emission tomography with magnetic resonance imaging. Proc. IEEE. **96**(3), 416–438 (2008)
142. Jarrett, B.R., Gustafsson, B., Kukis, D.L., Louie, A.Y.: Synthesis of (64)cu-labeled magnetic nanoparticles for multimodal imaging. Bioconjug. Chem. **19**(7), 1496–1504 (2008). https://doi.org/10.1021/bc800108v
143. Lee, H.-Y., Li, Z., Chen, K., Hsu, A.R., Xu, C., Xie, J., Sun, S., Chen, X.: PET/MRI dual-modality tumor imaging using arginine-glycine-aspartic (RGD)–conjugated radiolabeled Iron oxide nanoparticles. J. Nucl. Med. **49**(8), 1371–1379 (2008). https://doi.org/10.2967/jnumed.108.051243
144. Cai, W., Chen, K., Li, Z.B., Gambhir, S.S., Chen, X.: Dual-function probe for PET and near-infrared fluorescence imaging of tumor vasculature. J. Nucl. Med. **48**(11), 1862–1870 (2007). https://doi.org/10.2967/jnumed.107.043216
145. Phillips, E., Penate-Medina, O., Zanzonico, P.B., Carvajal, R.D., Mohan, P., Ye, Y., Humm, J., Gönen, M., Kalaigian, H., Schöder, H., Strauss, H.W., Larson, S.M., Wiesner, U., Bradbury, M.S.: Clinical translation of an ultrasmall inorganic optical-PET imaging nanoparticle probe. Sci. Transl. Med. **6**(260), 260ra149-260ra149 (2014). https://doi.org/10.1126/scitranslmed.3009524
146. Xie, R., Peng, X.: Synthesis of Cu-doped InP nanocrystals (d-dots) with ZnSe diffusion barrier as efficient and color-tunable NIR emitters. J. Am. Chem. Soc. **131**(30), 10645–10651 (2009)

147. Wang, H.-F., He, Y., Ji, T.-R., Yan, X.-P.: Surface molecular imprinting on Mn-doped ZnS quantum dots for room-temperature phosphorescence optosensing of pentachlorophenol in water. Anal. Chem. **81**(4), 1615–1621 (2009)
148. Santra, P.K., Kamat, P.V.: Mn-doped quantum dot sensitized solar cells: a strategy to boost efficiency over 5%. J. Am. Chem. Soc. **134**(5), 2508–2511 (2012)
149. Fang, M., Peng, C.-w., Pang, D.-W., Li, Y.: Quantum dots for Cancer research: current status, remaining issues, and future perspectives. Cancer Biol. Med. **9**(3), 151–163 (2012). https://doi.org/10.7497/j.issn.2095-3941.2012.03.001
150. Bourlinos, A.B., Bakandritsos, A., Kouloumpis, A., Gournis, D., Krysmann, M., Giannelis, E.P., Polakova, K., Safarova, K., Hola, K., Zboril, R.: Gd(iii)-doped carbon dots as a dual fluorescent-MRI probe. J. Mater. Chem. **22**(44), 23327–23330 (2012). https://doi.org/10.1039/C2JM35592B
151. Nie, L., Wang, S., Wang, X., Rong, P., Ma, Y., Liu, G., Huang, P., Lu, G., Chen, X.: In vivo volumetric Photoacoustic molecular angiography and therapeutic monitoring with targeted plasmonic nanostars. Small. **10**(8), 1585–1593 (2014). https://doi.org/10.1002/smll.201302924
152. Xu, M., Wang, L.V.: Photoacoustic imaging in biomedicine. Rev. Sci. Instrum. **77**(4), 041101 (2006). https://doi.org/10.1063/1.2195024
153. Mallidi, S., Luke, G.P., Emelianov, S.: Photoacoustic imaging in cancer detection, diagnosis, and treatment guidance. Trends Biotechnol. **29**(5), 213–221 (2011). https://doi.org/10.1016/j.tibtech.2011.01.006
154. Laufer, J., Johnson, P., Zhang, E., Treeby, B., Cox, B., Pedley, B., Beard, P.: In vivo preclinical photoacoustic imaging of tumor vasculature development and therapy. J. Biomed. Opt. **17**(5), 056016 (2012). https://doi.org/10.1117/1.jbo.17.5.056016
155. Zhang, H.F., Maslov, K., Sivaramakrishnan, M., Stoica, G., Wang, L.V.: Imaging of hemoglobin oxygen saturation variations in single vessels in vivo using photoacoustic microscopy. Appl. Phys. Lett. **90**(5), 053901 (2007). https://doi.org/10.1063/1.2435697
156. Wang, Z., Huang, P., Jacobson, O., Wang, Z., Liu, Y., Lin, L., Lin, J., Lu, N., Zhang, H., Tian, R., Niu, G., Liu, G., Chen, X.: Biomineralization-inspired synthesis of copper sulfide–ferritin nanocages as cancer theranostics. ACS Nano. **10**(3), 3453–3460 (2016). https://doi.org/10.1021/acsnano.5b07521
157. McCarthy, J.R.: The future of theranostic nanoagents. Nanomedicine. **4**(7), 693–695 (2009). https://doi.org/10.2217/nnm.09.58
158. Liang, K., Liu, F., Fan, J., Sun, D., Liu, C., Lyon, C.J., Bernard, D.W., Li, Y., Yokoi, K., Katz, M.H., Koay, E.J., Zhao, Z., Hu, Y.: Nanoplasmonic quantification of tumour-derived extracellular vesicles in plasma microsamples for diagnosis and treatment monitoring. Nat. Biomed. Eng. **1**, 0021 (2017). https://doi.org/10.1038/s41551-016-0021 http://www.nature.com/articles/s41551-016-0021#supplementary-information
159. Maiti, S., Sen, K.K.: Bio-Targets and Drug Delivery Approaches. CRC Press LLC, Boca Raton, FL, USA (2016)
160. Chow, E.K.-H., Ho, D.: Cancer nanomedicine: from drug delivery to imaging. Sci. Transl. Med. **5**(216), 216rv214-216rv214 (2013). https://doi.org/10.1126/scitranslmed.3005872